IVYSPRING INTERNATIONAL PUBLISHER

Theranostics

2021; 11(16): 7948-7969. doi: 10.7150/thno.61621

Review

3D bioprinting in cardiac tissue engineering

Zihan Wang[1,4]*, Ling Wang[3]*, Ting Li[1], Sitian Liu[1], Baolin Guo[5], Wenhua Huang[1,2]✉, Yaobin Wu[1]✉

1. Guangdong Engineering Research Center for Translation of Medical 3D Printing Application, Guangdong Provincial Key Laboratory of Medical Biomechanics, Department of Human Anatomy, School of Basic Medical Sciences, Southern Medical University, Guangzhou, 510515, China.
2. Guangdong Medical Innovation Platform for Translation of 3D Printing Application, Southern Medical University, The third Affiliated Hospital of Southern Medical University, Southern Medical University, Guangzhou, 510515, China.
3. Biomaterials Research Center, School of Biomedical Engineering, Southern Medical University, Guangzhou, 510515, China.
4. The First School of Clinical Medicine, Southern Medical University, Guangzhou, 510515, China.
5. Frontier Institute of Science and Technology, and State Key Laboratory for Mechanical Behavior of Materials, Xi'an Jiaotong University, Xi'an, 710049, China.

* These authors contributed equally to this work.

✉ Corresponding authors: Tel.: +86-020-61648086. Fax: +86-020-61648524. E-mail: wuyaobin2018@smu.edu.cn, huangwenhua2009@139.com

Received: 2021.04.14; Accepted: 2021.06.06; Published: 2021.07.06

Abstract

Heart disease is the main cause of death worldwide. Because death of the myocardium is irreversible, it remains a significant clinical challenge to rescue myocardial deficiency. Cardiac tissue engineering (CTE) is a promising strategy for repairing heart defects and offers platforms for studying cardiac tissue. Numerous achievements have been made in CTE in the past decades based on various advanced engineering approaches. 3D bioprinting has attracted much attention due to its ability to integrate multiple cells within printed scaffolds with complex 3D structures, and many advancements in bioprinted CTE have been reported recently. Herein, we review the recent progress in 3D bioprinting for CTE. After a brief overview of CTE with conventional methods, the current 3D printing strategies are discussed. Bioink formulations based on various biomaterials are introduced, and strategies utilizing composite bioinks are further discussed. Moreover, several applications including heart patches, tissue-engineered cardiac muscle, and other bionic structures created *via* 3D bioprinting are summarized. Finally, we discuss several crucial challenges and present our perspective on 3D bioprinting techniques in the field of CTE.

Key words: 3D bioprinting; bioinks; printed biomaterials; cardiac muscle; tissue engineering

Introduction

Cardiovascular diseases are highly prevalent diseases worldwide in terms of morbidity and mortality, especially in developed countries [1]. One out of every seven deaths is caused by coronary artery disease, and the estimated yearly incidence of myocardial infarction (MI) is 790,000 [1–3]. The adult human heart is the least regenerative organ in the body due to the limited regeneration capacity of cardiomyocytes (CMs) [4, 5], which means the heart cannot repair itself after injury [6]. Although various therapy strategies, such as heart stents and coronary bypass surgery, have been implemented in the clinic, reversing myocardial deficiencies remains an ongoing challenge. Cardiac tissue engineering (CTE) aims to develop functional engineered tissues and organs as *in vivo* transplants to alleviate the shortage in organs for transplantation or as *in vitro* models for research on disease mechanisms and drug discovery [7–9]. The native heart is a muscular organ that pumps blood through the blood vessels of the circulatory system [10]. The wall of the heart is composed of three layers: epicardium, myocardium, and endocardium (from the outside to the inside). The myocardium contains multiple anisotropic layers of CMs and collagen fibers with a gradual transition in orientations across its transmural depth, which contributes to the unique biomechanical behavior of cardiac tissue (**Figure 1**) [11]. The myocardium contains 2–4 billion aligned CMs (roughly 75% of the heart volume) although they represent only about 33% of the total cell number [12].

In addition, CMs associate with other types of cells, including endothelial cells (ECs), smooth muscle cells, and fibroblasts (FBs), to generate an intricately organized 3D structure [13]. Cardiac muscle also contains specialized cells that rapidly conduct electrical signals called Purkinje cells. Coronary arteries and countless capillaries are also present to nourish thicker cardiac tissues [14]. Thus, native cardiac muscle tissue is a relatively complicated system containing many features. Therefore, engineered cardiac tissue requires, at minimum, active cardiac cells with precise cell alignment and a 3D extracellular environment with specific cardiac structure and involvement of non-myocyte cells.

In the past decade, many studies have proved that prepared 3D culture environments are closer to *in vivo* conditions than conventional 2D culture techniques (Petri dishes) [15]. Many bioengineering techniques have been developed to generate elaborate and functional engineered cardiac tissue including micropatterning [16], electrospinning [17], and 3D bioprinting (3DBP). 3DBP is regarded as an especially promising technique for fabricating biomimetic scaffolds with the complex 3D structures required for cell proliferation and differentiation in various tissue engineering applications. Previous studies have reviewed 3DBP for cardiovascular regeneration and CTE applications including the development of printing parameters and bioink materials [18, 19]. In this review, we first briefly summarize published studies in CTE based on traditional scaffold fabrication techniques, and then demonstrated 3DBP would be beneficial for overcoming the drawbacks of the traditional CTE scaffolds. Subsequently, we describe various 3DBP strategies, biomaterials-based bioinks, and cell sources for 3DBP CTE. We also highlight the current application of 3DBP in CTE. Finally, we discuss the major challenges of current 3DBP strategies, describe future trends, and provide our perspective on the potential of bioprinted cardiac constructs for advancing research and clinical applications.

Overview of cardiac tissue engineering (CTE)

Tissue engineering scaffolds play a key role in CTE applications because they offer a supportive framework and provide a promotive micro-environment for cell adhesion, proliferation, and differentiation. The following scaffold properties are important for CTE applications: (i) Biocompatibility: scaffolds should show low immunogenicity and coagulability when implanted *in vivo*. (ii) Biodegradability: the transplanted scaffolds should be degraded *in vivo* by hydrolysis, oxidation, enzymes, or physical degradation. (iii) Mechanical strength: scaffolds should retain the shape with muscle tissue-like stiffness (~10 kPa) [21]. (iv) Bioactivity: scaffolds should enhance cell adhesion with high activity and promote cell proliferation and differentiation. Excellent scaffolds mimic the cellular components and specific micro-environment of the native tissue, such as its cell arrangement, micro-extracellular matrix (ECM) composition, and physical properties [22–24]. (v) Electrical conductance: scaffolds should allow the engineered constructs to perform the dynamic functions of the heart [25]. (vi) Anisotropy: scaffolds should have an anisotropic microstructure, which has been shown to promote CM alignment and favor cell differentiation and functionality [26–30].

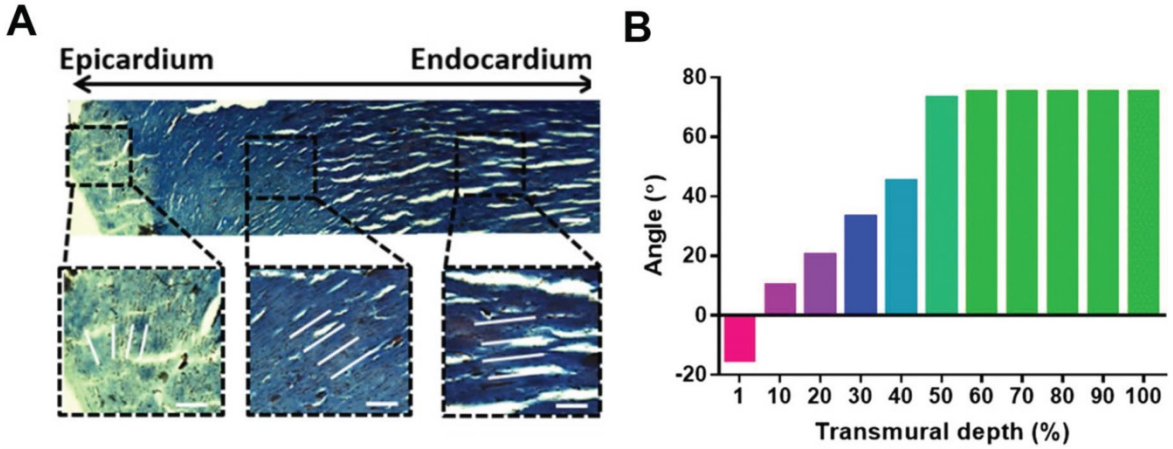

Figure 1. Adult rat hearts were harvested, sliced, and stained for cells and collagen to analyze variations in the transmural orientation. (A) Masson's trichrome staining of a transmural block cut from the ventricular wall showing the macroscopic variation in fiber orientation across the wall. (B) Analysis of collagen fiber orientation revealed that the degree of alignment from the epicardial side to the endocardial side had a 100° shift. Adapted with permission from [20]. Copyright 2017, National Academy of Sciences.

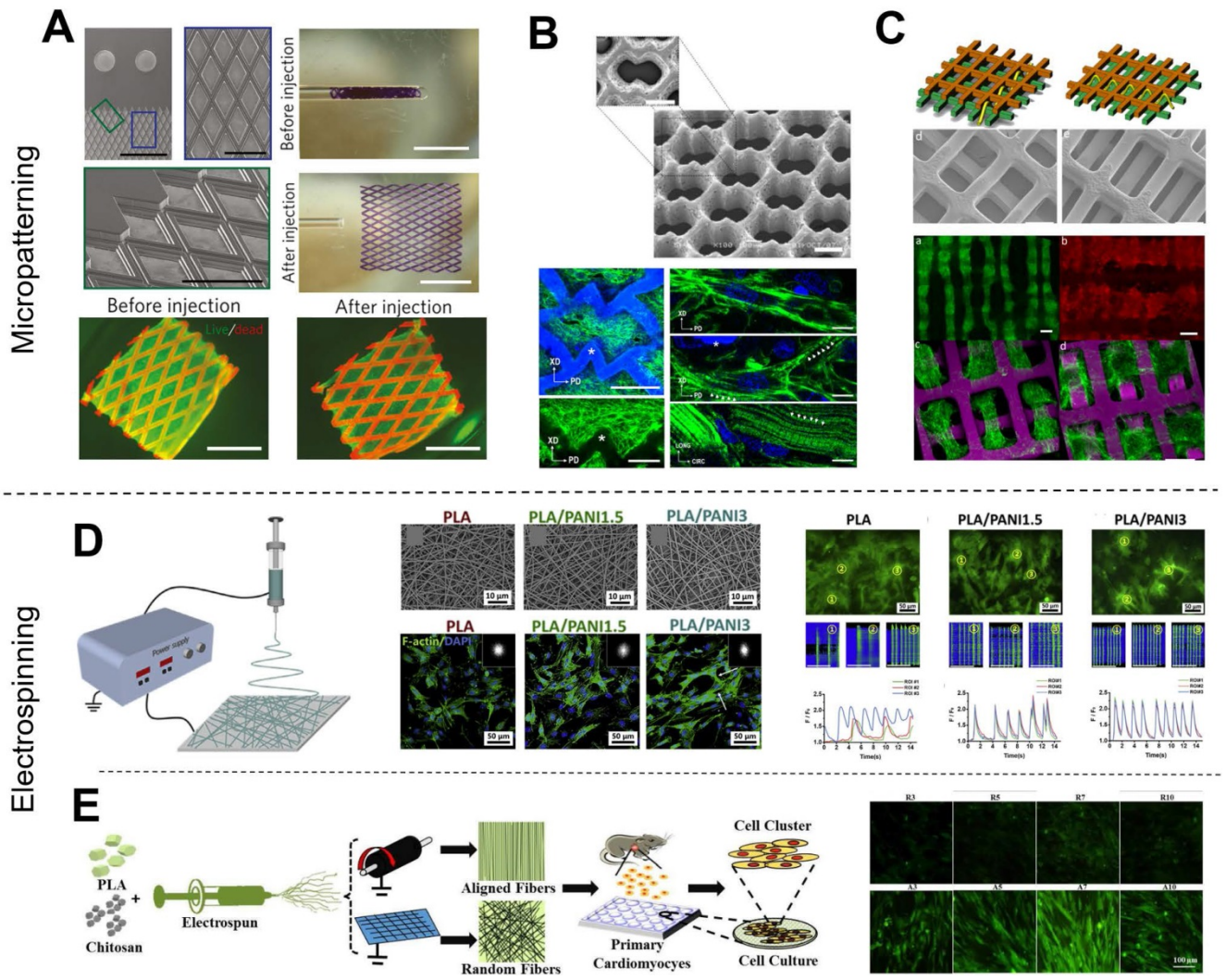

Figure 2. Traditional fabrication methods in CTE. (A–C) Examples of micropatterned scaffolds fabricated from bioelastomers. (A) Grid-patterned scaffold for myocardial repair prepared on a polydimethylsiloxane (PDMS) mold. Adapted with permission from [37]. Copyright 2017, Springer Nature. (B) Accordion-like honeycomb CTE scaffolds fabricated by excimer laser microablation. Adapted with permission from [38]. Copyright 2008, Springer Nature. (C) Multi-layered micropatterned elastic CTE scaffold fabricated using a microelectromechanical technique and packaging approach. Adapted with permission from [39]. Copyright 2013, John Wiley & Sons. (D–E) Examples of electrospun nanofibrous scaffolds for CTE applications. (D) Conductive electrospun nanofibrous sheet based on poly(L-lactic acid)/polyaniline. The scaffold promoted the maturation and spontaneous beating of primary CMs. Adapted with permission from [48]. Copyright 2017, Elsevier. (E) Random or aligned electrospun nanofibrous mats based on PLLA/chitosan. These scaffolds showed promise as platforms for regenerating myocardia and drug screening applications. Adapted with permission from [35]. Copyright 2017, Elsevier.

Various methods have been developed to fabricate scaffolds that induce cell orientations including micropatterning [16, 31–34], and electrospinning [17, 28, 35, 36]. Micropatterning is a simple and effective technique to fabricate anisotropic patterns for cell alignment. Various scaffold micropatterns have been developed for CTE applications, such as grids (**Figure 2A**) [37], accordion-like honeycombs (**Figure 2B**) [38], and even multi-layered patterns (**Figure 2C**) [39]. In particular, our previous study showed that micropatterned electroactive bioelastomer films (groove/ridge = 50 μm/50 μm) were able to significantly guide the elongation and alignment of primary CMs, and increased the intercellular concentration of Ca^{2+} compared with flat films [16]. Other studies [40, 41] have applied honeycomb microstructures as CTE scaffolds because cardiac muscle fibers are surrounded and coupled by endomysial collagen sheaths that are bundled within a honeycomb-like network of undulated perimysial collagen fibers [42]. Compared to square and rectangular patterns, honeycomb patterns generated scaffolds with higher ultimate tensile strength and strain to failure [41, 43]. Additionally, electrospinning is an excellent technique for fabricating nanofibrous scaffolds for CTE [44]. Electrospinning generates scaffolds with excellent mechanical properties and provides easy manipulation of fiber properties, great material handling, and scalable production. Studies have reported that fibers with decreased diameter facilitate cell adhesion and spreading [45] because cell membranes with embedded receptors can easily wrap around sub-micron-scale fibers [46, 47]. We

previously reported that electrospun conductive nanofibrous sheets were able to enhance cell-cell interactions, maturation, and spontaneous beating of primary CMs (**Figure 2D**) [48]. Also, available electrospinning collectors enable the production of a variety of nanofibrous constructs [36]. For example, flat collectors are used to generate random fibers while high-speed rotating drum and mandrel collectors are used to generate aligned fibers (**Figure 2E**) [48–50]. In our other previous studies, we used a developed dry–wet electrospinning method to develop a list of aligned nanofiber yarn (NFY) [34, 51]. In summary, these published studies based on micropatterning and electrospinning techniques demonstrated induction of cell alignment on 2D substrates or pseudo-3D environments. However, recapitulating the 3D organized cellular architecture of native heart tissues using these techniques remains challenging [6].

Hydrogel matrix systems present a 3D environment similar to that of native tissues, and cells can be encapsulated within hydrogel matrices homogeneously. Moreover, external stimulation approaches such as mechanical stimulation or electrical stimulation have been applied to control 3D cell alignment and elongation within hydrogel scaffolds [52–55]. However, the inconvenience of these external stimulation methods limits their application [56–58]. Shin *et al.* [59] presented an interesting method for engineering 3D multi-layered constructs using layer-by-layer assembly of cells separated by self-assembled graphene oxide-based thin films (**Figure 3A**). This multi-layered construct showed strong spontaneous beating and frequency-dependent opening/closing actuation under a low external electric field. However, CMs within the structure presented a random orientation, which is detrimental to heart contraction. In contrast, we previously developed core-shell scaffolds with electrospun aligned nanofiber yarns (NFYs) as the core and hydrogel as the shell that not only induced cell alignment and elongation but also provided a suitable 3D environment for cellular nutrient exchange and mechanical protection [34]. Furthermore, we designed an interwoven NFYs/hydrogel core-shell scaffold that controlled cell alignment and elongation according to the complex interwoven structure of native cardiac tissue, and then stacked cell-laden NFYs *via* layer-by-layer assembly with a slight angular shift to mimic the gradual transition in alignment between myocardium layers (**Figure 3B**) [11]. Similarly, Fleischer *et al.* [20] fabricated albumin micro-grooved scaffolds *via* electrospinning and laser patterning to engineer aligned cardiac tissues, and then stacked several of these grooved scaffolds with a slight angular shift (**Figure 3C**). Unfortunately, this layer-by-layer stacking strategy significantly increases the complexity of cell culture, and precise 3D cell and matrix organization is limited. In contrast, 3D printing showed the advantages for fabricating scaffolds with 3D complex structure, and these drawbacks of the traditional scaffolds are now being overcome by computer-assisted 3DBP [60].

3D bioprinting techniques for engineered cardiac tissue

3DBP, which similar to traditional 3D printing, is also an additive manufacturing technique but the printed inks or resins are replaced with cells only or biomaterials and cells mixture [61, 62]. 3DBP spatially controls the deposition of bioinks, allowing for the fabrication of functional living constructs with 3D customized architecture. Recent advancements have enabled several novel printing strategies.

3D bioprinting approaches

Inkjet printing

2D inkjet printers are modified for 3DBP by replacing the ink cartridge with biological material and adding an electronically controlled elevator stage for z-axis movement (**Figure 4A**). Inkjet bioprinting devices are classified into two types including thermal [63] and piezoelectric ones [64, 65]. Thermal-based printers produce pressure pulses and eject droplets by localized heating, while piezoelectric-based printers generate acoustic waves. The heat and acoustic waves have a negligible impact on cell viability [66, 67]. Inkjet bioprinting is compatible with many biomaterials and can maintain remarkable cell viability (> 90%) [68]. Boland's group used modified inkjet printers to fabricate contractile cardiac hybrids in the form of 3D rectangular sheets and half hearts [69, 70]. Moreover, the cardiac hybrid materials were tailored in 3D to achieve desired porosities and mechanical and chemical properties. However, considering its operating principle, inkjet-based bioprinting works with bioinks having a specific viscosity (3.5–12 mPa/s) [61], which usually leads to weak mechanical support [65]. To overcome this physical limitation, a post-crosslinking strategy has been introduced [71, 72]. Nevertheless, inkjet printers cannot still print cells at high densities, which is critical for creating cardiac constructs [73, 74].

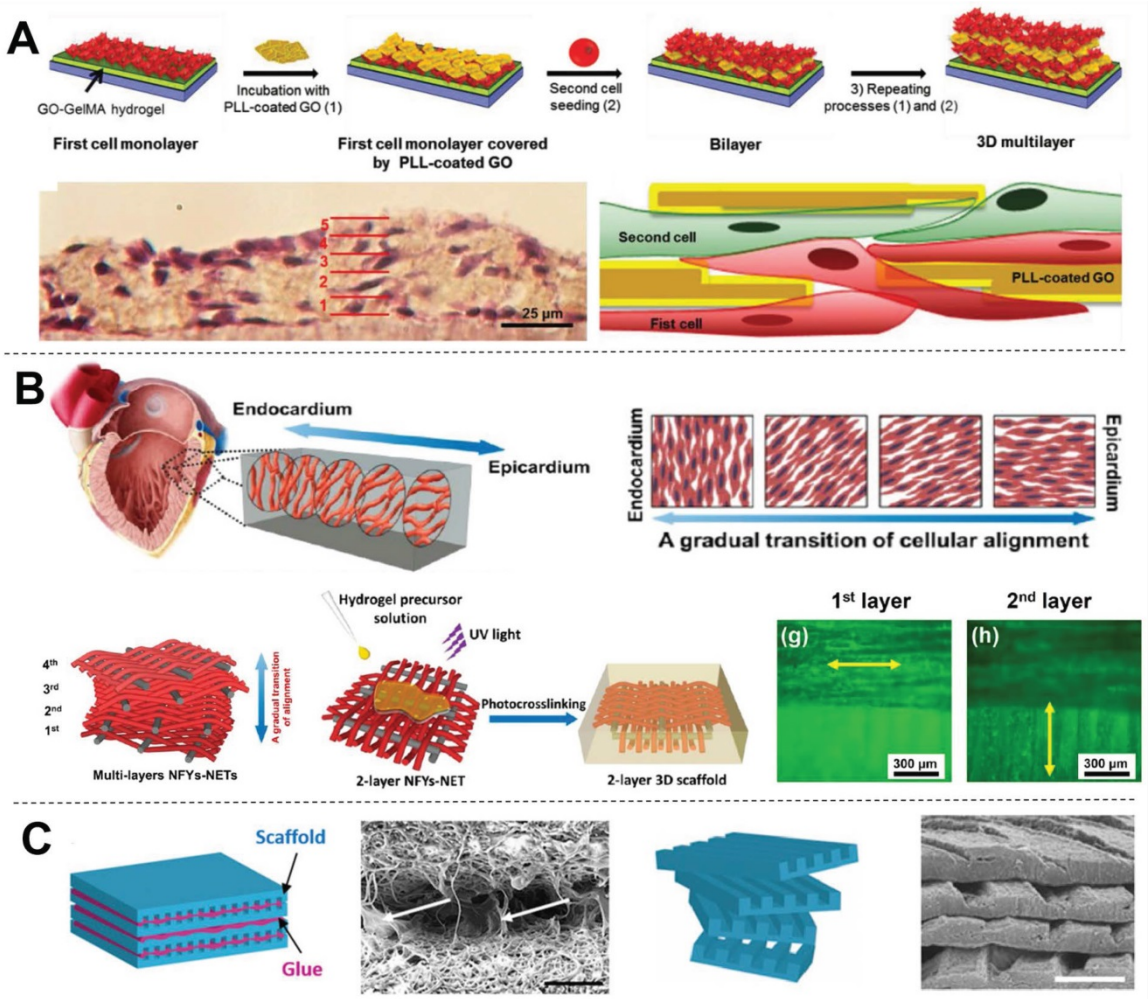

Figure 3. Examples of 3D CTE scaffolds with multi-layered structures (A) Multi-layer 3D CTE scaffold fabricated *via* layer-by-layered deposition of cardiac cells and graphene oxide (GO)-coated poly-L-lysine (PLL) films. Adapted with permission from [59]. Copyright 2014, John Wiley & Sons. (B) Multi-layered NFYs/hydrogel core-shell scaffold within a transition in the 3D orientation of CMs. Adapted with permission from [11]. Copyright 2017, American Chemical Society. (C) Grooved electrospun scaffolds stacked with a slight angular shift for guiding the orientation of multi-layered CMs. Adapted with permission from [20]. Copyright 2017, National Academy of Sciences.

Digital light processing printing

In digital light processing (DLP) printing, a digital micromirror array device is used to selectively solidify photocurable bioinks in a layer-by-layer process controlled by a moveable stage along the z-axis (**Figure 4B**) [75]. The main advantage of DLP printing is its simple and rapid manufacturing process. As the entire layer is printed simultaneously, the motion of the printer head in the x–y direction is avoided. This nozzle-free approach also avoids clogging and excessive shear stress to cells. Furthermore, it provides a higher resolution (50–100 μm) than the other printing strategies [6]. Liu *et al.* [76] encapsulated neonatal mouse ventricular CMs within a photocurable hydrogel by a DLP printing approach. The encapsulated CMs were aligned with the printed microarchitecture and showed observable force trace after various stimulation frequencies *in vivo*, which indicated that the rapid DLP printing approach was able to fabricate complex CTE scaffolds. However, several limitations still need to be overcome to apply DLP printing to CTE. First, biomaterials used for DLP printing must be photocurable; however, UV light exposure potentially damages cell DNA during the 3D printing process [77]. In addition, cell settling or sedimentation during DLP bioprinting also should be discussed, particularly when a thick scaffold is needed for printing. Chan *et al.* [78] found that, in a typical DLP printing approach, cells mixed within the bioresin settled to the bottom of the bioresin reservoir during printing, which created an inhomogeneous cell distribution within the printed construct. To overcome this challenge, Lin *et al.* [79] matched the buoyant density of the cells by adding 37.5% (v/v) Percoll to a poly(ethylene glycol) (PEG)-based bioresin to prevent cell settling. Moreover, it remains challenging to utilize multiple types of bioinks in DLP printing [80]. In comparison, extrusion printing can be used to easily fabricate constructs of multiple cells/materials by equipping two or more printer

heads [81]. However, a multiple bioresin reservoirs strategy is not suitable for DLP printing because of inevitable cross pollution between the reservoirs.

Extrusion printing

Extrusion printing uses pneumatic- or mechanical-driven fluid dispensing systems to constantly extrude bioink onto a platform (**Figure 4C**), which permits faster, simpler, and more affordable bioprinting compared with other techniques. Moreover, the deposited cell densities could be high and close to physiological CM densities (10^8–10^9 cells mL^{-1}), which is particularly crucial for CTE [73, 74]. However, the dispensing pressures and shear stresses applied to cells are significant and may result in poor cell survival (40–80 % cell viability) when extruding materials with high viscosity (> 6×10^7 mPa s) or when a thin nozzle is used [82, 83]. One study showed that cardiac myocytes are more sensitive to extrusion pressure than cardiac fibrocytes [84]. Therefore, shear-thinning hydrogels have been developed to overcome this limitation. Unlike conventional Newtonian bioinks, shear-thinning bioinks show significantly decreased viscosity with increasing strain rate during printing, which protects the cells from high shear stresses. For example, gelatin and its derivate materials as well as some decellularized ECM (dECM) hydrogels [74] are shear-thinning bioinks that are widely used in 3DBP for tissue engineering.

Freeform reversible embedding printing

Hydrogels are excellent candidates for supporting cell proliferation in 3D environments. However, most hydrogels suffer from poor mechanical properties, which potentially results in a collapse during printing of hollow structures due to gravity [85]. Thus, direct printing of hydrogels and other soft biomaterials (e.g., dECM) remains challenging. To overcome this limitation, Feinberg *et al.* [86] developed a strategy to extrude hydrogel bioink into another hydrogel as a support medium, which they called freeform reversible embedding (FRE) of suspended hydrogels (FRESH) (**Figure 4D**). The support bath in this strategy was composed of gelatin microparticles and acted like a Bingham plastic during printing. Bingham plastics behave as a rigid body at low shear stresses but flow as a viscous fluid at high shear stresses. This meant that there was little mechanical resistance when a needle-like nozzle moved through the bath, yet hydrogel extruded out of the nozzle and deposited within the bath was held in place. Thus, printed soft materials maintained the intended 3D geometry in this support bath. After solidification, the printed scaffold was easily taken out by melting the support bath (**Figure 5A**). In a subsequent study, Feinberg's group decreased the size of the gelatin microparticles in the support bath from ~65 μm to 25 μm and renamed the system FRESH v2.0 (**Figure 5B**) [85]. The diameters of the printed collagen filaments reliably decreased from 200 μm to 20 μm when FRESH v2.0 was used. Moreover, a porous microstructure was present after the gelatin microspheres were removed from the 3D-printed scaffold, which promoted cell infiltration and micro-vascularization [87]. Recently, various hydrogel materials have been developed as support media based on this strategy. For example, Edri *et al.* [88] printed two homocentric hollow spheres and a small hand in xanthan gum as the support bath (**Figure 5C**). Hinton *et al.* [89] printed helical and tubular structures in a Carbopol support gel (**Figure 5D**). FRE printing also has great potential for the fabrication of complicated structures. For example, Bhattacharjee *et al.* [90] printed a continuous knot in Carbopol support gel (**Figure 5E**). Even a whole neonatal-scale human heart has been successfully printed [85]. However, the conditions of the support bath (e.g., temperature, pH, ion concentration) might affect cell activity, especially prolonged printing. Another limitation is that the integrity of delicate structures and the viability of sensitive cells may be jeopardized by the mechanical force needed to remove the support medium [91]. Thus, compatible support baths are still very limited in variety.

Bioink preparation

Various biomaterials have been applied as bioinks for CTE applications recently **(Table 1)** [101, 102]. Usually, bioinks are made of hydrogel or polymer and cells are encapsulated into the bioinks or seeded on bioprinted constructs to promote cardiac tissue growth. The chosen biomaterials should be printable, which indicates their suitability for the fabrication of stable 3D constructs with high structural integrity and fidelity. Therefore, the mechanical properties of bioinks (e.g., modulus, rheology) are fundamental. In general, bioinks should provide a constant, precise deposition, followed by rapid, nontoxic solidification. These are key factors affecting resolution, cell viability, and post-print function, although each printing strategy has a few differences in detail [102–104]. The chosen biomaterials must also shield cardiac cells against varying levels of pressure and shear stress developed during printing processes [105]. Biomaterials also need to mimic the ECM of the human heart tissue to promote cell proliferation and differentiation [74]. Generally, biomaterials used as bioinks are grouped into natural and synthetic materials [106].

Table 1. Examples of biomaterials fabricated by various 3DBP techniques for cardiac and microvascular tissue engineering applications.

Bioink composition	Bioprinting technique	Cell resource	*In vitro/in vivo* results	Reference
Collagen	FRE Printing	C2C12/ hESC-CMs	High resolution (20 μm) and cell viability (96%). Suspended or hollow structures, such as the neonatal heart, were fabricated directly. Printed scaffolds exhibited micro-porous structures, which were beneficial to vascularization.	Feinberg *et al.* [85,86]
Alginate	Extrusion Printing	HCAECs	Interstrand distance and strand alignment angle in the 3D-printed pattern influenced stiffness, electrical conductivity, and porosity.	Izadifar *et al.*[92]
Gelatin	Extrusion Printing	Neonatal rat CMs/hMSCs	3D-printed microchannels induced hMSC orientation and myocardial lineage commitment, which improved the organization and rhythmic beating of CMs.	Tijore *et al.*[60]
GelMA	DLP Printing	Neonatal rat CMs	Cell shape and orientation in 3D were controlled by engineering scaffold microstructures and encapsulating cells near these geometric cues. Well-aligned myofiber cultured patterns generated 4-10 times the contractile force of less anisotropically patterned constructs.	Liu *et al.*[76]
GelMA	Extrusion Printing	Neonatal rat CMs/CFBs	CM-laden GelMA bioink was significantly more sensitive to extruder pressure than CFB-laden bioinks The ability of CM-laden constructs to form networks was affected by GelMA concentration.	Koti *et al.*[84]
PEGDA	DLP Printing	iPSC-CMs	Microscale continuous optical printing (μCOP) was optimized to achieve miniaturization and promote cardiac tissue maturation. Demonstrated potential for high-throughput *in vitro* drug screening	Ma *et al.*[93]
PCL/CNT	Extrusion Printing	H9c2	Incorporation of CNTs reinforced the alignment of polymer chains, resulting in a slight enhancement in crystallinity, due to interactions with the PCL matrix. PCL-CNT nanocomposites with 1%(w/w) CNT showed optimal conductivity and stiffness for the proliferation of H9c2 cells.	Ho *et al.*[94]
PGS/nanocellulose/PPy	Extrusion Printing	H9c2	These cardiac patches fulfilled the requirement of the highly dynamic and functional electroresponsive cardiac tissue given their biocompatibility, biodegradability, mechanical strength, flexibility, and electrical conductivity. The slow degradation of the cardiac patches indicated their suitability for long-term drug release.	Ajdary *et al.*[95]
PCL/hdECM	Extrusion Printing	hCPCs/hMSCs	hdECM might potentiate epicardial-mediated cardiac tissue regeneration followed by migration of Wilms tumor protein 1 positive progenitor cells via epithelial-mesenchymal transition. This 3D pre-vascularized stem cell patch effectively delivered the stem cells *via* the epicardial delivery route.	Jang *et al.*[81]
Alginate/PEG/fibrinogen	Extrusion Printing	iPSC-CMs/HUVECs	Bioprinted endothelial cells effectively developed vasculature in transplanted cardiac tissues, and integrated with the host vasculature.	Maiullari *et al.*[96]
Alginate /MeCol/CNTs	Extrusion Printing	HCAECs	Incorporation of CNTs in MeCol significantly improved the electrical conductivity of the hydrogel and improved cell attachment and elongation. CNTs reinforced hydrogel crosslinking in alginate.	Izadifar *et al.*[97]
GelMA/hdECM	Extrusion Printing	hCPCs/rat-CFBs	Incorporation of hdECM within patches resulted in a 30-fold increase in the cardiogenic gene expression of hCPCs compared to hCPCs grown in pure GelMA patches. Conditioned media from GelMA-hdECM patches show increased angiogenic potential (>2-fold) over pristine GelMA. Patches were retained on rat hearts and showed vascularization over 14 d *in vivo*.	Bejleri *et al.*[98]
GelMA/alginate	Extrusion Printing	Neonatal rat CMs/HUVECs	A microfluidic perfusion bioreactor was designed to complete an endothelialized myocardium-on-a-chip platform for cardiovascular toxicity evaluation.	Zhang *et al.*[99]
GelMA/hdECM	Inkjet Printing	iPSC-CMs/human-CFBs	The viabilities of cells before and after printing were almost equivalent. High-density 3D tissues (3.5×10^8 cells cm^{-3}) with high cell viability (92.8 ± 1.5%) were produced	Chikae *et al.*[100]

Natural biomaterials as bioinks

Among the various natural biomaterials, heart-derived dECM (hdECM) is one of the most typic natural bioinks. dECM is obtained from the organ of interest by detergent treatment to remove cells, which preserves the ECM and maintains the architecture of cell-cell interactions (**Figure 6A**). Therefore, hdECM recapitulates most of the chemical cues of native heart tissue to promote cell survival, differentiation, and functionality [107]. Jang *et al.* [81] transplanted a cell-free hdECM-based heart patch in the epicardium of a rat MI model to assess the functional benefits of hdECM materials for tissue repair. Less adverse remodeling was observed in the hdECM group than in the blank control group. In contrast, eccentric remodeling of the heart was observed in the control group seven days after implantation. However, the therapeutic concentrations of dECM solution (6-10 mg mL^{-1}) had relatively low viscosity, and the bioprinted layers were hard to sustain their previously defined 3D structure. Although previous studies have developed some printing methods to overcome the poor printability of hdECM, there are still two main issues worth attention [74, 81]. First, the required concentration of hdECM solution (20 mg mL^{-1}) is significantly higher than that used in therapeutic studies, which is limiting because the preparation of hdECM requires extensive harvesting from porcine sources. Second, pure hdECM-printed structures are relatively hard to print and potentially rupture when applied as a patch for heart regeneration due to their low mechanical modulus and fibrous nature [108, 109]. Collagen, the major constituent of the ECM, is considered an excellent cell delivery platform for cardiac applications due to its ability to promote cell

adhesion and differentiation [110, 111]. More importantly, collagen is more readily available to most researchers than dECM. However, collagen also suffers the same printing and mechanical problems as dECM due to its low Young's modulus and viscosity [97]. To precisely control the mechanical properties of natural polymers, chemical conjugations of natural biomaterials have been developed [112]. For example, methacrylated type-I collagen (MeCol) is obtained by adding methacrylate to the amine-containing side groups of collagen (**Figure 6D**). Collagen provides cell adhesion molecules to ensure the required bioactivity, while methacrylate allows adjustable construct stiffness due to methacrylate photopolymerizability under UV light [97]. Similarly, gelatin methacryloyl (GelMA), another widely used material, is gelatin modified with a photopolymerizable methacrylamide group (**Figure 6C**) [107]. GelMA is mechanically tunable based on its degree of methacrylation, and its elastic modulus can be adjusted by altering its concentration and printing parameters such as printing temperature, duration of UV light exposure and type, and amount of photoinitiator [113, 114]. The choice of photoinitiator is important because every photoinitiator requires a different wavelength of light for crosslinking, and some wavelengths are potentially more damaging to cells. For instance, the suitable wavelengths for 1-[4-(2-hydroxyethoxy)-phenyl]-2-hydroxy-2-methyl-1-propan-1-one (Irgacure 2959) is 365 nm and for lithium phenyl(2,4,6-trimethylbenzoyl) phosphinate (LAP) is 405 nm, respectively. Luckily, a white light system (Eosin Y system) has been developed recently to initiate crosslinking in 5 min without causing any damage to cells [98, 115].

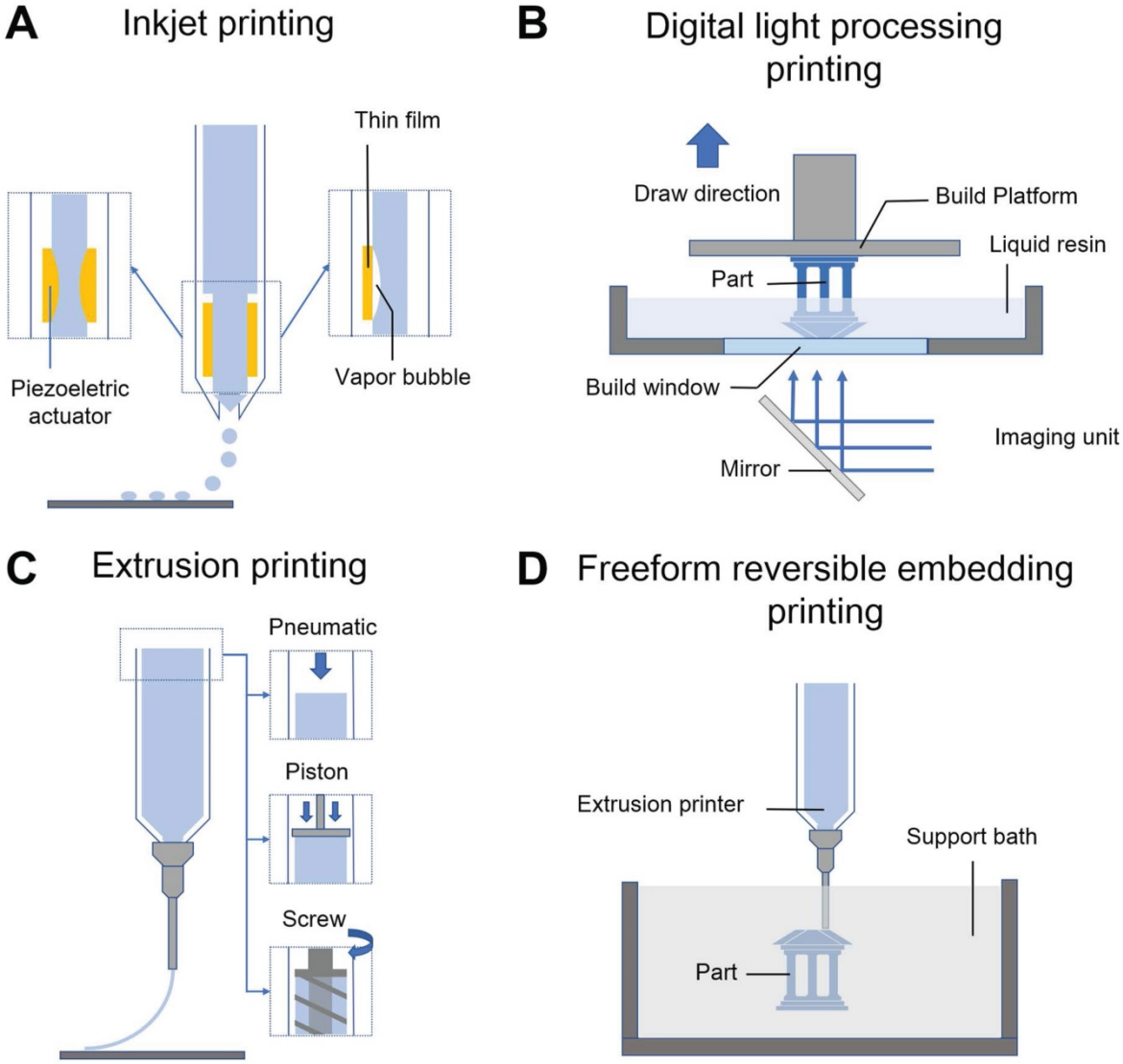

Figure 4. Schematic illustrations of various 3DBP technologies. (A) Inkjet printing: thermal or piezoelectric actuators are applied to form droplets of bioink-cell hybrids. (B) Digital light processing printing: ultraviolet or visible light is used to cure a photopolymer in a vat for layer-by-layer manufacturing of a 3D model. (C) Extrusion printing: pneumatic, piston, or screw forces are applied to extrude continuous beads of bioink. (D) Freeform reversible embedding printing: bioink is extruded into a reversible support bath for fabrication of support-free structures.

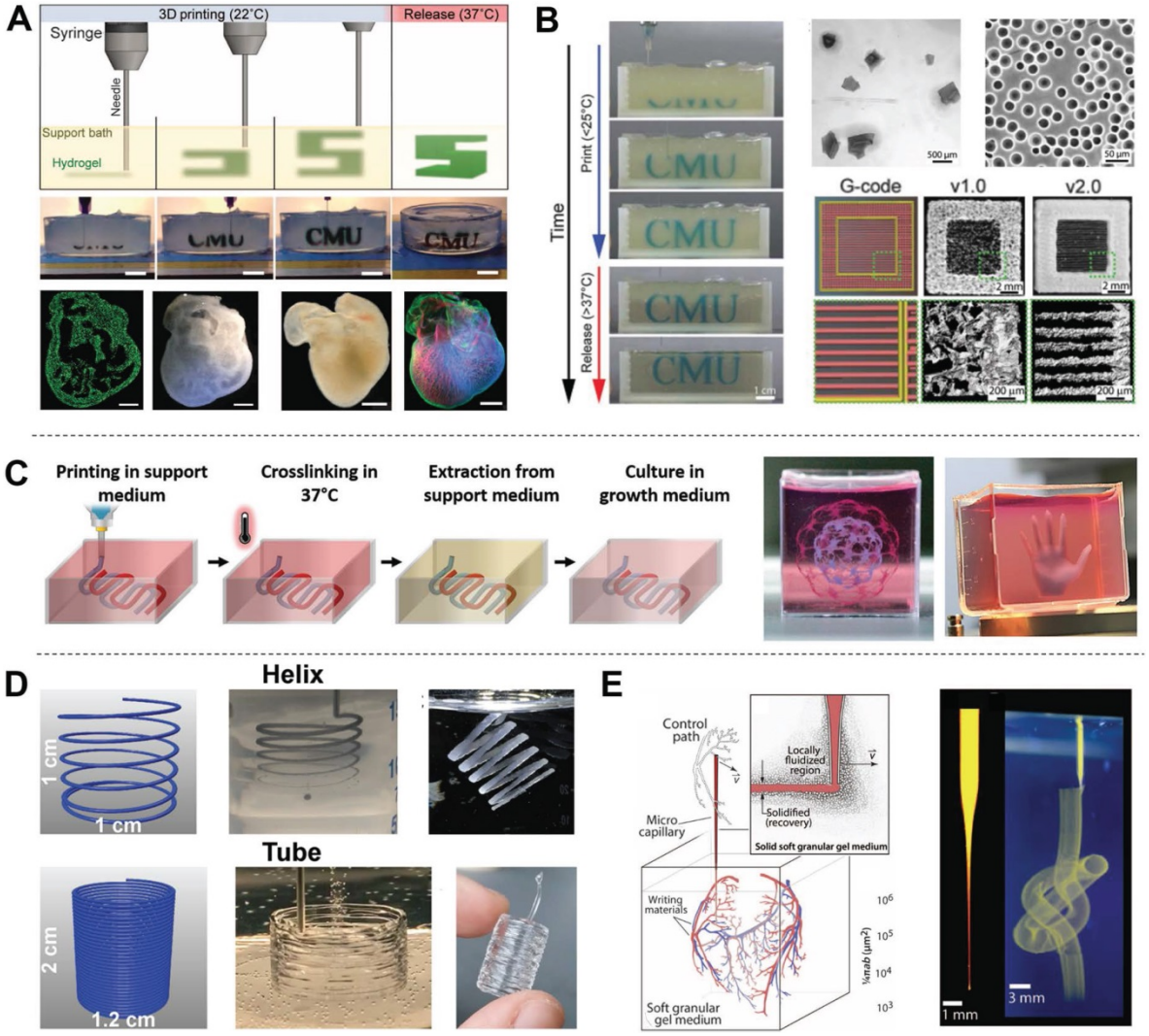

Figure 5. Examples of FRE printing strategies. (A) Schematic of the printing and crosslinking process of hydrogel (green) within a gelatin slurry support bath (FRESH v1.0). A whole neonatal-scale human heart was printed via FRESH v1.0. Adapted with permission from [86]. Copyright 2015, American Association for the Advancement of Science. (B) Gelatin microspheres with smaller diameter were used as the support bath in FRESH v2.0, resulting in printed structures with higher resolution. Adapted with permission from [85]. Copyright 2019, American Association for the Advancement of Science. (C) A xanthan gum support bath was shown to support complicated structures (hollow sphere, small hand). Adapted with permission from [91]. Copyright 2019, John Wiley & Sons. (D) Helical and tubular structures printed in Carbopol support gel by freeform extrusion. Adapted with permission from [89]. Copyright 2016, American Chemical Society. (E) A continuous knot of aqueous fluorescent microspheres in Carbopol support gel written without the simultaneous building of any other support structure. Adapted with permission from [90]. Copyright 2015, American Association for the Advancement of Science.

Synthetic biomaterials as bioinks

Synthetic polymers have also been widely used as bioinks in 3DBP for CTE applications (**Figure 6E**). In general, synthetic bioinks offer better physical integrity, higher mechanical strength, and enhanced printability compared with natural bioinks. Synthetic polymers potentially have controllable physico-chemical properties (e.g., degradation rate, diffusion rate, hydrophobicity) *via* adjustment of their molecular weight or post-printing management [6]. He *et al.* [118] fabricated microscale polycaprolactone (PCL) fibers with an average size of 9.5 μm by melt-based electrohydrodynamic (EHD) printing to mimic cardiac collagenous fibers, which guided layer-specific cell orientations. Poly (L-lactic acid) (PLLA) is one of the most extensively studied biodegradable polyesters. PLLA is degraded into water and carbon dioxide by hydrolysis or esterases in the body [119]. PLLA-based vascular scaffolds as cardiovascular implants are able to overcome the shortcomings associated with metallic implants, including restricted normal vasomotion and adaptive remodeling of the arterial vessel wall, and bypass surgery [120]. However, most synthetic hydrogels are brittle and lack flexibility and elasticity, making it difficult to mimic the softness, stretchability, and elasticity of human soft tissues, such as blood vessels and heart muscles. Xu *et al.* [117] designed a triblock copolymer, PCL-PEG-PCL diacrylate, as the single-component precursor to form a crosslinked hydrogel network (**Figure 6F**). This hydrogel exhibited high flexibility and elasticity, withstanding large deformations from stretching, compression, and

twisting without any obvious breakage, and recover quickly from deformation. However, the hydrophobic surface of synthetic polyesters prevents hydration and protein absorption, and the absence of Arg-Gly-Asp (RGD) peptides prevents cell attachment [121, 122]. To overcome these limitations, chemical grafting of synthetic polymers has been developed. For example, Costantini *et al.* [123] formulated a tailored bioink with a photocurable semi-synthetic biopolymer (PEG-fibrinogen) that is composed of denatured fibrinogen fragments with covalently attached PEG side chains having a vinyl moiety at their extremities. Shape memory polymers (SMPs) have also been applied to design smart scaffolds. SMPs have the ability to return from a deformed state to their original (permanent) shape when induced by an external stimulus. For example, shape memory polyurethane is widely used to fabricate smart robots or injectable scaffolds because it has controllable structure performance with a tunable shape memory temperature range (-30 to 70 °C) [124]. Radisic *et al.* [37] designed an elastic and microfabricated scaffold for functional tissue delivery via injection. Scaffolds and cardiac patches (1 cm × 1 cm) were delivered through an orifice as small as 1 mm and recovered their initial shape following injection without affecting cardiomyocyte viability and function. Xiao *et al.* [125] fabricated a self-adhesive conductive cardiac patch from SMPs to promote electrical signal transduction and improve function in the MI area. Shape memory has shown great potential for invasive delivery via tiny orifices and smart biomedical robots.

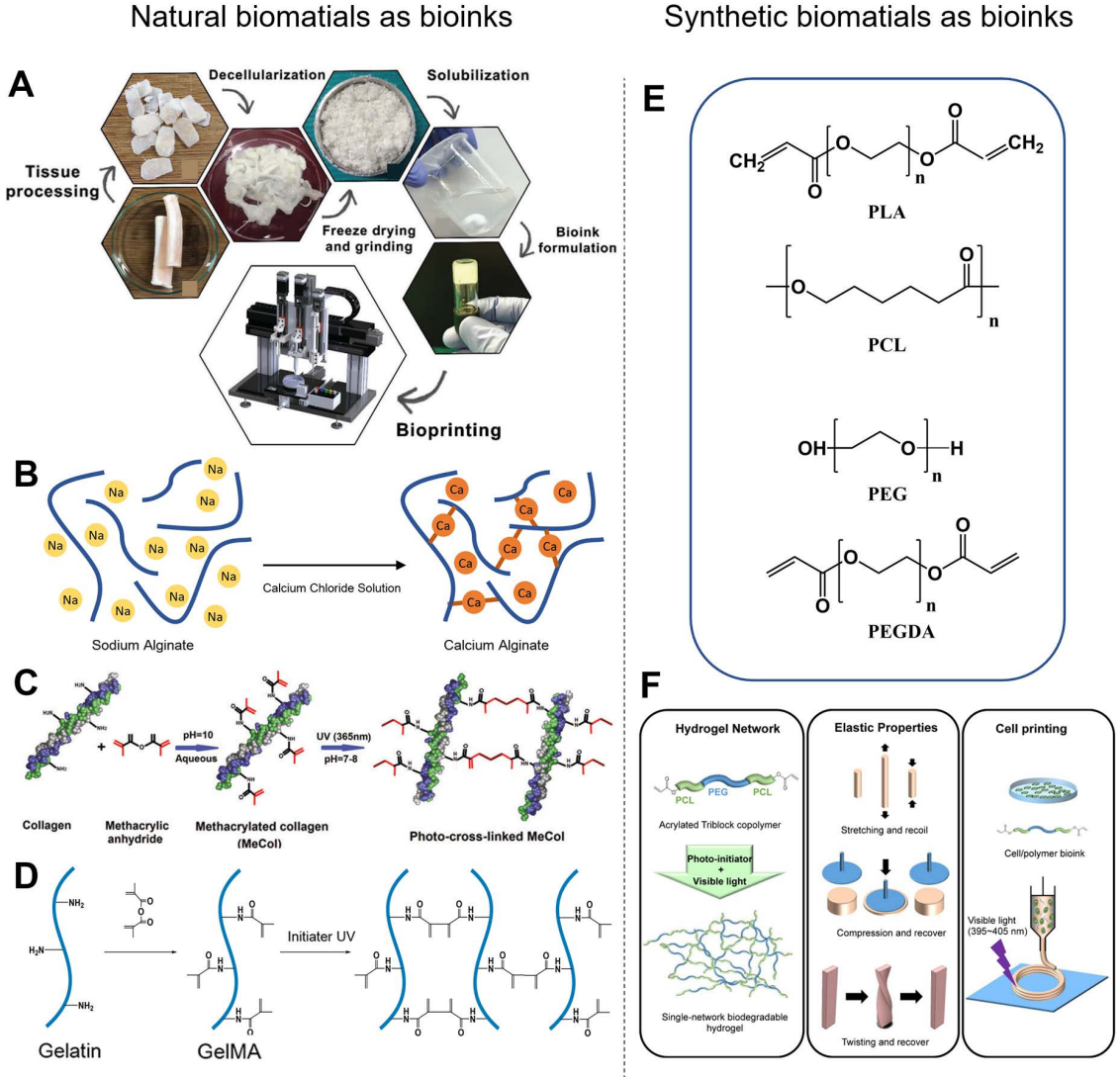

Figure 6. Examples of natural and synthetic biomaterials applied as bioinks. (A) Schematic diagram of the process for preparing dECM bioink. Adapted with permission from [116]. Copyright 2018, John Wiley & Sons. (B) Schematic diagram of alginate calcium-induced crosslinking. (C) Schematic diagram of GelMA formation and UV light-induced crosslinking. Adapted with permission from [97]. Copyright 2018, Mary Ann Liebert. (D) Schematic diagram of MeCol formation and UV light-induced cross-linking. (E) Chemical structures of synthesized polymers commonly used in 3DBP. PLA, polylactic acid; PCL, polycaprolactone; PEG, poly(ethylene glycol); PEGDA, poly(ethylene glycol) diacrylate. (F) Schematic diagram of acrylated PCL-PEG-PCL triblock polymer synthesis, and simple gelation into single-network hydrogel using visible light. Adapted with permission from [117]. Copyright 2018, American Chemical Society.

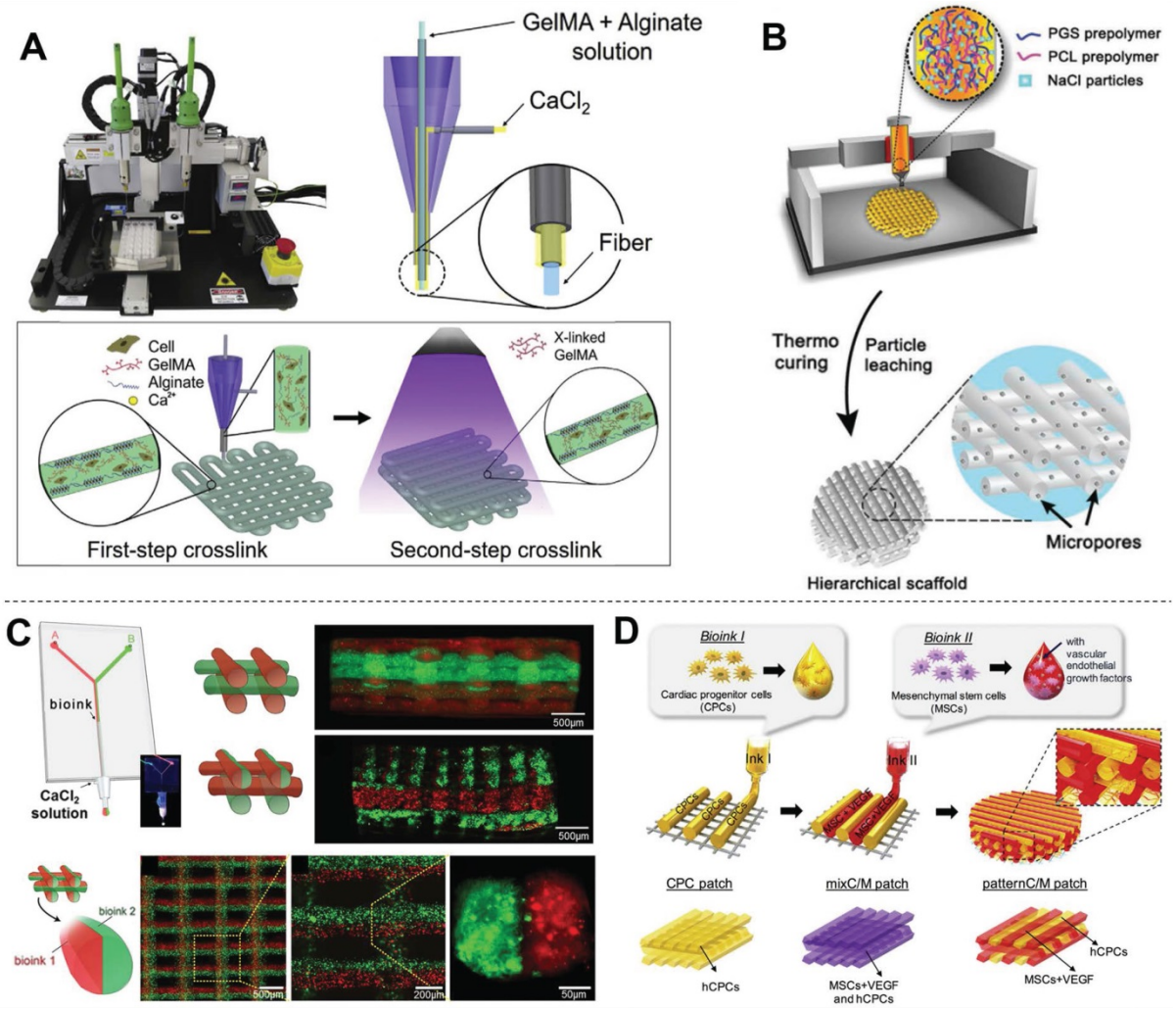

Figure 7. Preparation of hybrid bioinks for 3DBP in CTE. (A) Schematic diagram showing the two-step crosslinking process for alginate-GelMA hybrid bioinks, The alginate component was first physically crosslinked by $CaCl_2$ then GelMA was chemically crosslinked *via* UV illumination to stabilize the 3D printed scaffolds. Adapted with permission from [99]. Copyright 2016, Elsevier. (B) Schematic diagram illustrating how salt particles can be used as a temporary mechanical support and to facilitate thermoplastic processes, including fused deposition modeling (FDM) 3D printing. Adapted with permission from [135]. Copyright 2019, John Wiley & Sons. (C) Schematic diagram of a microfluidic system used to flow two bioinks (containing red and green fluorescent beads) that exited the device through a single extruder. This device opened new routes for the creation of complex and heterogeneous tissue fibers on demand. Adapted with permission from [133]. Copyright 2015, John Wiley and Sons. (D) Schematic diagram of a multi-printer system used to fabricate pre-vascularized stem cell patches from multiple cell-laden bioinks and supporting PCL polymer. The printed dual stem cell structure improved cell-to-cell interactions and cell differentiation and promoted functionality for tissue regeneration. Adapted with permission from [81]. Copyright 2017, Elsevier.

Hybrid bioinks

Hybrid bioinks refer to any permutation of multiple natural or synthetic polymers. Since every biomaterial has merits and faults, hybrid bioinks aim to combine strengths and circumvent weaknesses to form more suitable bioinks for 3DBP. Most hybrid bioinks take advantage of the cell-supportive properties of natural polymers and the mechanical properties and tunability of synthetic polymers. For example, PCL is a widely used biomaterial in 3DBP, but its lack of bioactivity reduces cell affinity and the high hydrophobicity leads to low tissue regeneration rates [126]. One solution to overcome these limitations is to add nanoparticles, such as carbon nanotubes (CNTs) [127]. Kim *et al.* [94] found that H9c2 cells grown on PCL/CNT composite scaffolds had a higher proliferation rate than those grown on pure PCL scaffolds. This result indicated that the inclusion of CNTs might provide more favorable conditions for the adhesion and proliferation of H9c2 cells. Grafting hydrophilic fragments of synthetic or natural polymers such as acrylates, collagen, and chitosan, to hydrophobic biomaterials has also been explored [128–132]. In another study, Bejleri *et al.* [98] combined hdECM with GelMA hydrogel to bioprint cardiac patches for heart repair. The inclusion of hdECM improved the differentiation and reduced the proliferation of neonatal human cardiac progenitor cells (hCPCs) compared with GelMA alone, which in turn may improve the paracrine potential of hCPC-laden GelMA-hdECM patches. Some hybrid bioinks are mixed from multiple biomaterials for optimization of their mechanical properties to for

3DBP. One such strategy involves a second crosslinking reaction to prepare a double-network hydrogel. Alginate crosslinking system is widely used to prepare double-network hydrogels by exploiting the ability of alginate to undergo instantaneous gelation when exposed to Ca^{2+} [123]. Moreover, alginates are easily dissolved in the absence of calcium ions. Khademhosseini *et al.* [99] mixed alginate with GelMA (a low-viscosity bioink) to form a hybrid bioink for 3DBP using a coaxial needle (inner: GelMA-alginate bioinks; outer: crosslinker solution) (**Figure 7A**). Instantaneous gelation of the hybrid bioink took place at the tip of the inner needle; therefore, the GelMA-alginate bioink was capable of generating self-supported multi-layered structures. The scaffold was further treated with UV irradiation for photocrosslinking, which improved its structural stability. Colosi *et al.* [133] printed GelMA-alginate following a similar strategy, forming a fully interconnected mesh of deposited fibers that were stacked without signs of vertical collapse. Another strategy is to use nanoparticles as rheology modifier to tune the mechanical properties of the cell-laden fibers to mimic the morphological and mechanical features of native tissue and induce cell spreading. For example, Zhu *et al.* [134] used gold nanorods as a rheology modifier to adjust GelMA bioink. The adjusted gold nanorod-GelMA hydrogel had a Young's modulus of 4.2 ± 0.3 kPa, which was higher than that of pristine GelMA hydrogel (3.75 ± 0.15 kPa) and was adequate for its envisaged application in cardiac tissue implant. You *et al.* [135] adjusted the mechanical properties of poly(glycerol sebacate) (PGS) for stability and ease of extrusion by adding salt particles. The salt was used both as a temporary mechanical support during printing and curing and as a water-soluble porogen for introducing hierarchical micropores. This solution addressed the incompatibility of PGS with typical thermoplastic processes due to its harsh curing conditions of high temperature and high vacuum. In a subsequent study, PGS/PCL/salt composites were printed into cardiac patches with various viscoelastic properties for heart regeneration (**Figure 7B**) [136]. Another strategy is to print several bioinks separately using a microfluidic system (**Figure 7C**) or multi-printer devices (**Figure 7D**). The printed synthetic polymers are usually used as support frameworks, which allows mechanically weaker bioinks to be printed on top [81]. Meanwhile, Separately printed materials have also been utilized as sacrificial materials to support special hollow structures. For example, Wang *et al.* [137] utilized PCL as the framework, a fibrin-based composite hydrogel as the bioink, and gelatin as the sacrificial material to print a 3D construct in the form of string. Separate dispensing modules were used for each type of hydrogel and PCL during 3D printing., The obtained cardiac tissue constructs showed a spontaneous synchronized beating in culture and a phenomenal response during *in vitro* drug screening studies.

Native myocardium is an electroactive tissue that spontaneously contracts under electric signal propagation [138, 139]. Thus, conductivity is an important property for CTE scaffolds. Khademhosseini *et al.* [134] observed that CMs on gold nanorod-incorporated GelMA scaffolds synchronous exhibited beating on day 2, which was much earlier than CMs cultured on pristine GelMA hydrogel (day 5). Currently, various additive conductive materials have been explored to recapitulate the conductivity of native myocardium in CTE. For instance, CNTs are interesting candidate substrates or additives for CTE scaffolds due to their mechanical and electrical properties [140, 141]. Izadifar *et al.* [97] bioprinted hybrid cardiac patches from MeCol and alginate. CNT-reinforced hybrid constructs presented significantly higher stiffness and electrical conductivity as well as remarkable growth, proliferation, migration of human coronary artery endothelial cells (HCAECs) over 7 days of culture. In another study, Ho *et al.* [94] mixed CNTs with PCL to print hybrid scaffolds. Incorporation of CNTs reinforced the alignment of the polymer chains, resulting in a gradual enhancement in elastic modulus and hardness as well as slight enhancement in crystallinity, due to interactions with the PCL matrix. PCL-CNT nanocomposites with 1%(w/w) CNT showed optimal conductivity for H9c2 cells, leading to a slight increase in their proliferation *in vitro*. In addition, polypyrrole (PPy), a heterocyclic conductive polymer [142], is an excellent candidate additive for CTE scaffolds, showing a host of advantages including stimulus responsiveness, *in vitro* and *in vivo* biocompatibility [143], appropriate chemical stability, large specific surface area, and easy surface modification for incorporation of bioactive molecules [144]. Ajdary *et al.* [95] reported drug-loaded printed conductive patches for heart repair based on PGS mixed with PPy and nanofibrillated cellulose. PPy facilitated both cytocompatibility and electrical conductivity (34 ± 2.7 mS cm^{-1}) [145] while PGS slowed the degradation of the cardiac patches, making them suitable for long-term drug delivery. In summary, recent advancements in CTE have employed various permutations of multiple natural or synthetic materials to control every property of bioinks in order to mimic native cardiac tissue. These trials have immensely enhanced the variety and possibility of 3DBP for CTE.

Cell resource

Various types of cells have been used in 3DBP for CTE (**Table 1**) including cell lines, primary myocardial cells, neonatal human cardiac progenitor cells, and stem cell-derived CMs. Established CM cell lines (HL-1, H9c2) are useful alternatives to primary cells for various CTE studies. The H9C2 cell line was originally derived from embryonic rat ventricular tissue [146]. H9c2 cells share many properties with primary CMs, including membrane morphology, G protein expression, and electrophysiological properties. However, H9c2 cells are not able to beat [147, 148]. In contrast, primary myocardial cells isolated from rat neonatal hearts are widely used to engineer functional cardiac muscle *via* 3DBP technology for regenerative medicine, drug screening, and potentially disease modeling [99]. Although primary myocardial cells are excepted to represent the real condition of heart tissue, there is an immunological mismatch between the graft and the host tissue due to the interspecies difference [149, 150]. Human neonatal c-KIT-expressing CPCs are harvested from the atrial appendage, which is obtained from pediatric patients aged one week or less undergoing heart surgeries due to congenital heart diseases [98]. Agarwal *et al.* [151] showed that progenitor cells could improve the failing right ventricle of neonatal rats subjected to pulmonary banding. However, both primary myocardial cells and hCPCs suffer from shortages in supply. To overcome these challenges, human pluripotent stem cells have been extensively investigated for CTE [152]. The stem cells are derived either from developing blastocysts (human embryonic stem cells; hESCs) or from reprogrammed somatic cells (induced pluripotent stem cells; iPSCs) through the addition of transcription factors including Klf-4, Oct 4, Sox 2, and c-Myc [152, 153]. These cells could generate unlimited numbers of various types of cells, including functional CMs. Moreover, iPSC-derived CMs have the advantage of overcoming ethical concerns [19]. They also allow for the development of personalized medicine with patient-specific implants or drugs because of their ability to proliferate [154], in contrast to the non-proliferating nature of primary CMs. Noor *et al.* [91] utilized iPSC-CMs to bioprint a fully personalized cardiac patch for therapeutic applications. The iPSCs were generated from patient omental stromal cells; therefore, the engineered patches would not provoke an immune response after transplantation, eliminating the need for immunosuppression therapy [88], and have great potential for drug screening in an anatomically appropriate structure. Human pluripotent stem cells are also a predominant source of adult human CMs for clinical therapeutics. However, iPSC-CMs still lack many essential features, such as defined organization and distribution as well as functional transverse tubules [155].

Native heart tissue is composed of multiple types of cells, that each plays a part in CTE. Although CMs are responsible for electrical conduction and generation of contractile force, single CM scaffolds fail to develop tissue constructs when they are cultured alone [156, 157]. It has been established that non-muscular heart cells, such as cardiac FBs (CFBs) and vascular ECs, also play a key role in myocardial function. For example, ECs are essential for the vascularization of constructs to match nutrient demands, and cocultures of CMs and ECs in 3D scaffolds were shown to result in functionalized cardiac tissue constructs with increased CM physiology and viability [19]. Maiullari *et al.* [96] biofabricated vascularized heart tissue implant with iPSC-CMs and ECs. The bioprinted ECs effectively developed vasculature in the transplanted tissues, which could potentially anastomose with the host vessels. CFBs make up 70% of the cells within the myocardium while only occupying a quarter of the tissue volume, providing essential structural support to CMs and producing most cardiac ECM proteins [158]. Many previous studies have formed small self-contracting cardiac muscle strips by combining these two cell populations to mimic the native heart components [159–161]. In another study, Arai *et al.* [162] mixed three types of cells to form cell spheroids with high cell densities for 3DBP. Cell spheroids formed from a 50:25:25 mixture of iPSC-CMs/human umbilical vein endothelial cells (HUVECs)/CFBs had a more generalized and homogenous expression pattern than spheroids formed with other cell ratios. By analyzing the time-lapse imaging of cardiac spheroid formation, the authors also demonstrated that the addition of CFBs and HUVECs promoted rapid cell self-organization and enhanced cardiac spheroid stability.

Applications of 3DBP in CTE

3DBP of heart patches

Left ventricular (LV) remodeling is a pathological process characterized by LV dilation and altered chamber geometry, which is attributable to CM deficiencies. These compensatory mechanisms temporarily ensure adequate cardiac output by increasing stroke volume, at the cost of changing the LV architecture and impairing cardiac contractility. However, CMs have a limited regenerative capacity, and the cardiac ECM is modified and replaced by scar tissue during the progression of heart failure [163]. Scar tissue is non-elastic, so it affects heart

contraction. Therefore, Heart patches aim to promote functional CMs migration for repairing heart deficiencies instead of scar tissue formation. Bejleri *et al.* [98] combined GelMA and cardiac ECM hydrogel scaffolds with hCPCs to fabricate heart patches with an infill pattern of 90° grids by extrusion printing for myocardial reconstruction. These bioprinted hCPCs had high cell viability and enhanced gene expression of early cardiac transcription factors and the sarcomeric protein troponin T during cell culture. Vessels formed in this patch 14 days after *in vivo* implantation, which indicated that this patch integrated with the native myocardium and allowed for nutrient delivery to the implanted cells. Ajdary *et al.* [95] prepared a 3D-printed curcumin-releasing heart patch from nanofibrillated cellulose, PGS (a representative bioelastomer), and PPy (a conductive polymer). The slow degradation of the cardiac patches was expected to prevent burst release of the drug, making them suitable for long-term drug delivery after MI. Furthermore, many studies have developed heart patches incorporating multiple cells *via* a multiple printer system. For example, Maiullari *et al.* [96] utilized two bioinks containing iPSCs-CMs or HUVECs, respectively, to develop vascularized heart tissue. Ameliorated vascularization was observed for the multi-cell bioprinted structures compared with the controls devoid of endothelial cells. Moreover, the spatial arrangement of the HUVECs played a role in vascularization, and a Janus construct developed a better performing vascular network that was integrated with the host than other printed patterns (**Figure 8A**). Park *et al.* [164] bioprinted a heart patch with human bone marrow-derived mesenchymal stem cells (hBMSCs) and engineered hepatocyte growth factor–expressing MSCs (HGF-eMSCs) for improved vasculogenic potential and enhanced vascular regeneration in MI hearts. The authors further demonstrated that the primed hBMSCs survived longer within a cardiac patch and confirmed cardioprotection, evidenced by substantially higher numbers of viable CMs in the MI hearts. Elasticity is an important parameter of heart patches to match the demands of contractile tissue. You *et al.* [135] used PGS and PCL as a hybrid bioink to print an elastic heart patch for preserving infarcted myocardium. The 3D-printed PGS-PCL patches showed better performance in preserving heart function, reducing infarct size, and increasing heart wall thickness compared with single polymer patches prepared from PCL *or* PGS. In their subsequent study, You's group designed a perfusable, multifunctional epicardial device (PerMed) based on PGS/PCL *via* 3D printing with a subcutaneously implanted drug delivery system and showed the feasibility of minimally invasive surgical PerMed implantation in pigs, which also demonstrated its promise for clinical translation to treat heart disease [165] (**Figure 8B**). The microstructure or pattern also influences the properties of heart patches. Two microarchitectural features defined by the interstrand distance and strand alignment angle have been identified as major parameters for assessing the electrical/mechanical and structural behaviors of 3D-printed constructs [92]. An improper pattern design value usually leads to structurally unstable or lack of transverse conduction [166]. In summary, advanced cardiac patches should be considered based on their bioink components and pattern design, which determine regeneration-related properties, such as conductivity, modulus, nontoxicity, and even drug release.

3DBP of *ex vivo* cardiac muscle model

Ex vivo cardiac muscle models are one of the primary applications of CTE. They aim to facilitate research on the basic physiology of the heart or to serve as high-throughput drug screening platforms *in vitro*. Organized cell alignment is important for the realization of functional engineered cardiac muscle. Therefore, most CTE studies follow the principle that scaffolds should be designed to induce cardiac cell orientation. In particular, free-form 3DBP technologies allow for easy modification of the constructed pattern given their flexibility compared with other techniques. For example, Tijore *et al.* [60] bioprinted micro-channel patterned gelatin hydrogel scaffolds and then seed neonatal rat CMs on the scaffold for cultivation (**Figure 8C**). Elongated cells with significant βMHC expression (a differentiation-related gene) were observed on microchanneled scaffolds with 500 μm spacing. CMs on the microchanneled scaffolds showed more obvious spontaneous beating than those on plain scaffolds. Conversely, on wide microchanneled surfaces (~800 μm spacing), aligned cells contacting the channel edges tended to have less influence on cells adhered centrally and failed to confer any guidance cues [168, 169]. Recently, the concept of "organ-on-a-chip" has trended for its precise control of CTE. Organ-on-a-chip is a microfluidic cell culture device created by microchip manufacturing methods that contains continuously perfused chambers inhabited by living cells arranged to simulate tissue- and organ-level physiology [170]. Organ-on-a-chip devices might be more responsive to 3D cell-cell and cell-matrix interactions than *in vitro* 2D cell culture models, meaning they have great potential for drug screening. Moreover, organ-on-a-chip is expected to overcome limitations of traditional animal models such as high costs, time-consuming, and interspecies variation.

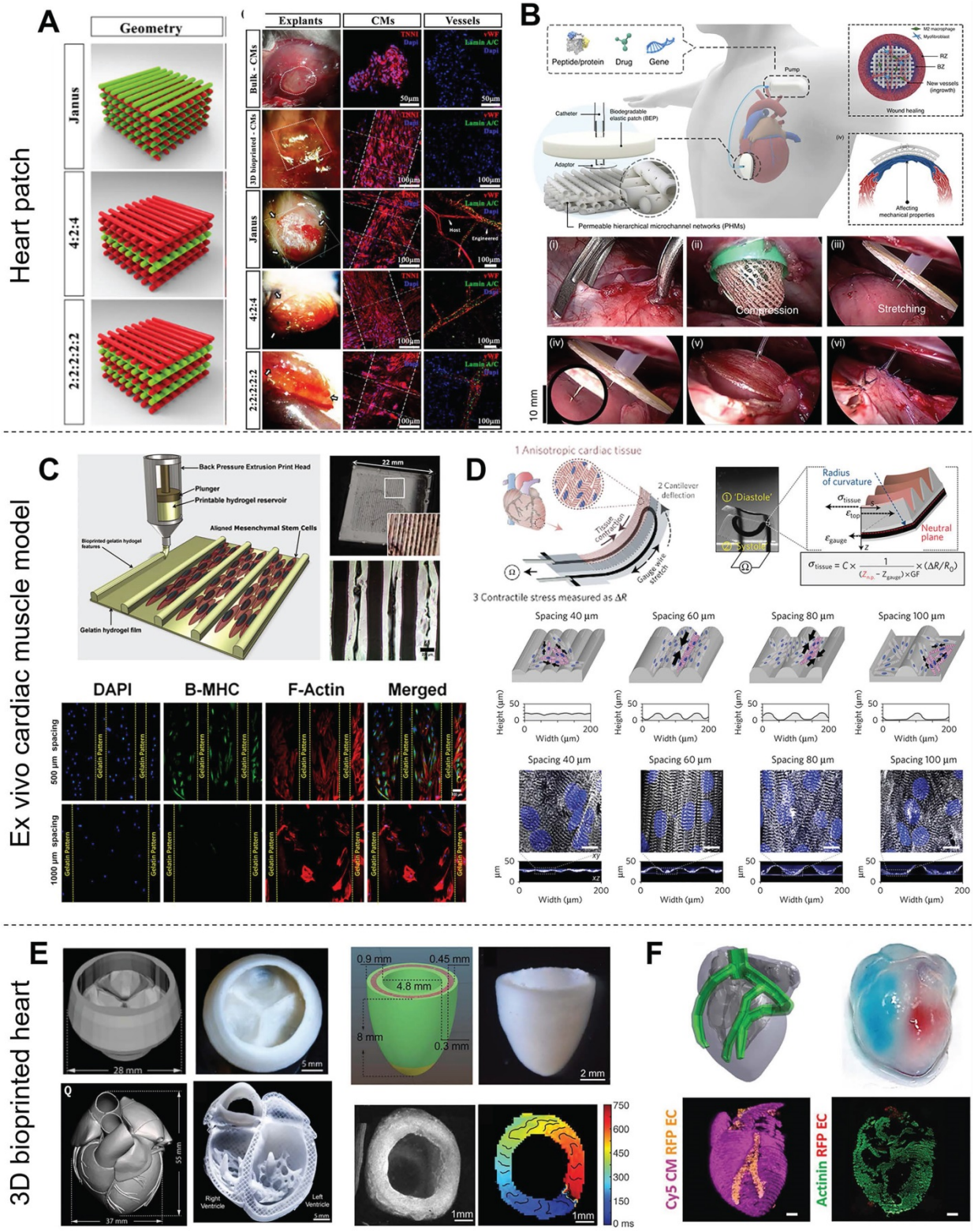

Figure 8. Various applications of 3D-bioprinted constructs for CTE. (A) Left: Schematic illustration of vascularized heart patches printed from iPSC-CM-laden bioink and HUVEC-laden bioink. Right: Representative images of patches after 7 days of culture showing expression of troponin I (red) and connexin 43 (green) in CMs and von Willebrand factor (green) in HUVECs, indicating that a well-developed vascular network was formed in the printed structures. Adapted with permission from [96]. Copyright 2018, Springer Nature. (B) Schematic illustration of the perfusable, multifunctional epicardial device (PerMed) consisting of a biodegradable elastic patch, permeable hierarchical microchannel networks and a system to enable delivery of therapeutic agents from a subcutaneously implanted pump (top). The process of PerMed implantation in pigs *via* laparoscopic surgery (bottom). Adapted with permission from [165]. Copyright 2021, Springer Nature. (C) Top: Schematic illustration and electron microscopy images of bioprinted microchanneled hydrogels with variable spacing. Bottom: Fluorescence microscopy images assessing the effect of the hydrogels on the alignment, elongation, and differentiation of hMSCs. Adapted with permission from [60]. Copyright 2018, IOP Publishing. (D) Design of a cardiac muscle chip with a stress sensor to monitor muscle contraction for applications in drug screening. Adapted with permission from [167]. Copyright 2016, Springer Nature. (E) Images of an organ-scale tri-leaflet heart valve (top left), a neonatal-scale human heart (bottom left), and a human cardiac ventricle model (right) printed by FRE, showing the capability of this strategy for precise deposition of bioink. Adapted with permission from [85]. Copyright 2019, American Association for the Advancement of Science. (F) Schematic illustration (top left) and photograph (top right) of a heart printed within a support bath and 3D confocal images (bottom) showing its robust structure and perfusable. Adapted with permission from [91]. Copyright 2019, John Wiley & Sons.

Furthermore, the cells in organ-on-a-chip allow for the use of patient-derived iPSCs for tailoring of medical compounds to individual patients [171]. However, the need for multiple parameter readouts is a burden on sample analysis. In particular, heart-on-chip requires detection of contraction and monitoring of many chemical combinations. Lind *et al.* [167] printed a sensor-studded cardiac tissue chip to easily monitor heartbeat through the change in electrical resistance. Carbon black nanoparticles were printed into the middle of the chip as an electronic sensor (**Figure 8D**); therefore, stress could be read by calculating the change in resistance, which was much more accessible and straightforward compared with microscopy coupled with optical tracking analysis. Other studies have induced an inverse opal structure to reveal the heartbeat by a change in color [172, 173]. These chips were treated with various concentrations of positive or negative inotropic drugs (e.g., isoproterenol) and showed a sensitive response to drug stimulation.

3DBP of engineered hearts

Engineering a whole heart organ with full functions comparable to native tissue is the ultimate goal of CTE to solve the short supply of donated organs. Thanks to the convenience of computer-assisted 3D printing technology, the heart computer-aided design (CAD) models of human hearts were developed from CT and MRI scans or downloaded from the model library. The parameters of the CAD models would be further tuned to make them suitable for 3DBP. However, printing an intact 3D structure with heart geometry is still challenging and is limited by the ability to combine multiple types of cells and fabricate multi-scale structures with different biomaterials. Recently, many elaborate structures have been bioprinted by FRE printing that mimics the macroscopic anatomical heart. For instance, Lee *et al.* [85] printed a tri-leaflet heart valve (28 mm in diameter), a neonatal-scale collagen heart, and a human cardiac ventricle model to demonstrate the precise deposition of their FRESH strategy (**Figure 8E**). The collagen tri-leaflet valve had well-separated leaflets and was robust enough to be handled in air. The authors quantified the flow through the valves and demonstrated <15% regurgitation. Furthermore, HUVECs cultured on unfixed collagen leaflets formed a confluent monolayer. Moreover, the microscale internal structure of the printed neonatal-scale collagen heart, such as trabeculae, matched the architecture defined in the G-code file. In another study, Noor *et al.* [91] printed hearts (height: 20 mm; diameter: 14 mm) from two bioinks containing Cy5-labeled CMs and ECs. The integrity of the different compartments was demonstrated by the injection of blue and red dyes (**Figure 8F**). Moreover, the mechanical properties of the printed hearts closely resembled the properties of decellularized rat hearts. One day after printing, high magnification of the cells comprising the printed heart showed a homogeneous distribution of CMs. In summary, recent developments in whole heart printing present the possibility for 3DBP with high-resolution and precise deposition of boinks. Additionally, the concept of FRE printing offers a theoretical basis on which to build up these complicated crafts, which might make it the most promising strategy for printing advanced tissue scaffolds for a wide range of organ systems [85].

Perspective and challenges

In the past decade, 3DBP has evolved to become more sophisticated, and some bioprinted human anatomical parts (e.g., ear, nose, hydroxyapatite bone substitutes) have already been used in the clinic [174–176]. Despite its significant progress and promise, 3DBP is still incapable of culturing a truly functional heart. One of the challenges is printing resolution. To closely mimic native tissue, bioink should be ideally deposited with a resolution comparable to cell size (5–10 μm). Additionally, to reach clinical applications, thick multi-layered muscle tissue is required. The maximum nutrient/oxygen diffusion distance for cells to survive without vascularization is ~100-200 μm [177]. However, it is still challenging to generate controlled vascular tree-like networks. The realization of vascularized CTE might be a barrier for another decade. In recent decades, bioprinting techniques for CTE have significantly developed in structural complexity, but bioprinting of soft materials (e.g., hydrogels) is still immature and many challenges remain [178]. Luckily, the emerging concept of using a reversible support bath to enable freeform reversible embedding of suspended hydrogels bioprinting is valid for most low-viscosity materials and makes it possible to print any complicated structure without the design of extra support [85]. However, the real heart organ has complex components comprised of multiple cell types, ECM, and multiscale structures for pumping blood, so further development of 3DBP strategies for CTE is needed.

Another research direction in 3DBP is the development of bioinks. Ideal bioinks should be printable, bioactive, biodegradable, stable, affordable, and commercially available with appropriate regulatory guidelines for clinical use [181]. However, currently available materials still have deficiencies in these respects. The development of hybrid bioinks is by far the best approach to developing high-quality bioinks. Moreover, smart materials and 4D printing

have attached great attention in research communities. In 4D printing, the shape, properties, or functionality of a 3D printed structure evolves overtime when it is exposed to a predetermined stimulus, such as heat [182, 183], humidity [184, 185], light [186, 187], or pH [188]. 4D structures can perform specific functions, such as self-folding, drug-releasing, or monitoring, which provide additional functions to scaffolds and generate a massive potential for multiple applications. Breakthroughs in SMPs and new printing control strategies [189] have underlain achievements in 4D printing. However, analysis of the structural mechanics of CAD models before printing is still deficient. In the future, finite element analysis [190, 191] and topology optimization [192], which are widely used in medical equipment design, could be employed to analyze these patches, hearts, and other models to allow for precise design of the material system for structure regulation, and performance optimization.

Another interesting area of research in CTE is the fabrication of 3D structures and functional tissues directly in live animals. For example, Urciuolo *et al.* [193] showed that intravital 3DBP of donor muscle-derived stem cells under the epimysium of hindlimb muscle in mice leads to *de novo* formation of myofibers. Intravital 3DBP takes advantage of commonly available multiphoton microscopes for the accurate positioning and orientation of the bioprinted structures into specific anatomical sites, which has enabled the fabrication of complex structures inside tissues of live mice, including the dermis, skeletal muscle, and brain. Intravital 3DBP might serve as an *in vivo* alternative to conventional bioprinting.

Another research trend in CTE is the combination of 3DBP with other biofabrication techniques. Since every printing technique has intrinsic shortcomings, 3DBP has been combined with other biofabrication techniques to benefit from their merit. For example, Maiullari *et al.* [96] combined 3DBP with microfluidic-based printer heads to achieve high-resolution bioprinting of heterogeneous constructs composed of iPSC-derived CMs and HUVECs with different spatial distributions, enabling the fabrication of 3D cardiac tissue models enriched with a vascular network (**Figure 9A**). Fukunishi *et al.* [179] combined 3DBP with electrospinning to create patient-specific nanofiber tissue-engineered vascular grafts (**Figure 9B**). The vascular grafts were implanted as an inferior vena cava interposition conduit in a sheep model. All sheep survived after 6 months without aneurysm formation or ectopic calcification, which indicated the clinical potential of the grafts. Castilho *et al.* [180] reported a melt-based EHD printing technique to deposit fibers with an average diameter of 10 μm to highly defined scaffold structures (**Figure 9C**). The printed cardiac scaffolds had highly organized fiber architectures with a rectangular pattern that promoted CPC alignment and were found to approximate the broad mechanical properties of native myocardial tissue. He *et al.* [118] applied EHD printing techniques to produce micron-scale PCL fibers and sub-micron conductive fibers to mimic the collagenous fibers and conductive Purkinje fibers in native cardiac ECM. CMs on the conductive scaffold showed enhanced synchronous beating compared with those on pure microfibrous scaffolds. Finally, with the rapid developments in bioprinting, common standards for additive manufacturing technologies should be established to normalize 3D-bioprinted products and access more opportunities for clinical trials of therapies.

Conclusion

3DBP is a promising technique for CTE owing to its ability to print heterogeneous structures and make full use of advanced achievements in cell and material engineering fields. Although there are still many challenges facing CTE for clinical applications, recent developments in printing strategies, such as emerging technologies, new bioinks, and better combinations of cells, will enable 3DBP to satisfy myriads of practical applications, including personalized drug screening, cardiac muscle reconstruction, and organ transplantation.

Abbreviations

hESC-CMs: human embryonic stem cell-derived cardiomyocytes; HCAECs: Human coronary artery endothelial cells; hMSCs: human mesenchymal stem cell; GelMA: gelatin methacryloyl; PEGDA: Poly (ethylene glycol) diacrylate; iPSC-CMs: induced pluripotent cell-derived cardiomyocytes; PCL: polycaprolactone; CNT: carbon nanotube; PGS: poly(glycerol sebacate); PPy: polypyrrole; hdECM: heart extracellular matrix hydrogel; hCPCs: Neonatal Human Cardiac Progenitor Cell; PEG: Poly (ethylene glycol); HUVECs: Human Umbilical Vein Endothelial Cells; MeCol: methacrylated collagen; CFBs: cardiac fibroblasts.

Acknowledgments

This work was supported by the National Natural Science Foundation of China (31972915, 31900960, and 32000955), the National Key R&D Program of China (2017YFC1103400), and the Guangdong Basic and Applied Basic Research Foundation (2019A1515011413).

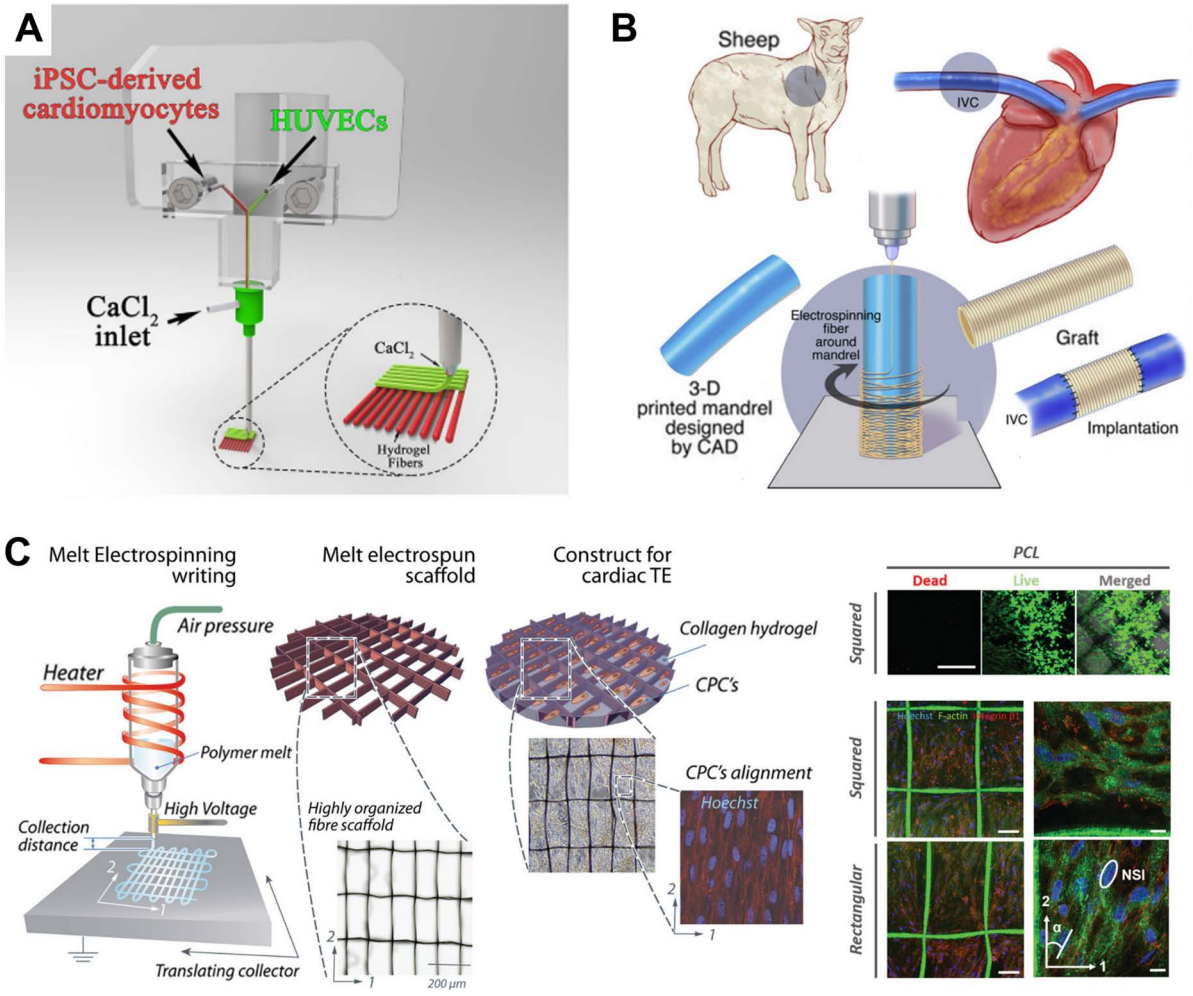

Figure 9. Examples of 3DBP strategies combined with other biofabrication techniques. (A) A microfluidic printing head guaranteeing high-resolution bioprinting generated heterogeneous constructs composed of iPSC-derived CMs and HUVECs with different spatial distributions, enabling fabrication of 3D cardiac tissue models enriched with a vascular network. Adapted with permission from [96]. Copyright 2018, Springer Nature. (B) 3DBP was combined with electrospinning to create patient-specific nanofiber tissue-engineered vascular grafts, which were effective in repairing inferior vena cava. Adapted with permission from [179]. Copyright 2016, Elsevier. (C) A custom-built melt electrospinning writing device enabled high-resolution (~10 μm) deposition of bioink (left) to print rectangular patterns that promoted CPC alignment (right). Adapted with permission from [180]. Copyright 2017, John Wiley & Sons.

Competing Interests

The authors have declared that no competing interest exists.

References

1. Roth GA, Johnson C, Abajobir A, Abd-Allah F, Abera SF, Abyu G, et al. Global, Regional, and National Burden of Cardiovascular Diseases for 10 Causes, 1990 to 2015. J Am Coll Cardiol. 2017; 70(1): 1-25.
2. Townsend N, Wilson L, Bhatnagar P, Wickramasinghe K, Rayner M, Nichols M. Cardiovascular disease in Europe: epidemiological update 2016. Eur Heart J. 2016; 37(42): 3232-45.
3. Benjamin EJ, Blaha MJ, Chiuve SE, Cushman M, Das SR, Deo R, et al. Heart Disease and Stroke Statistics-2017 Update: A Report From the American Heart Association. Circulation. 2017; 135(10): e146-e603.
4. Bergmann O, Bhardwaj RD, Bernard S, Zdunek S, Barnabé-Heider F, Walsh S, et al. Evidence for cardiomyocyte renewal in humans. Science. 2009; 324(5923): 98-102.
5. Kajstura J, Gurusamy N, Ogórek B, Goichberg P, Clavo-Rondon C, Hosoda T, et al. Myocyte turnover in the aging human heart. Circ Res. 2010; 107(11): 1374-86.
6. Serpooshan V, Mahmoudi M, Hu DA, Hu JB, Wu SM. Bioengineering cardiac constructs using 3D printing. J 3D Print Med. 2017; 1(2): 123-39.
7. Furman E. The dynamic state of patents in regenerative medicine. Tissue Eng Regen Med. 2013; 10(5): 230-3.
8. Mhashilkar AM, Atala A. Advent and maturation of regenerative medicine. Curr Stem Cell Res Ther. 2012; 7(6): 430-45.
9. Badylak SF, Nerem RM. Progress in tissue engineering and regenerative medicine. Proc Natl Acad Sci U S A. 2010; 107(8): 3285-6.
10. Venes D. Cyclopedic Medical Dictionary. 20th ed. Philadelphia: F. A. Davis Company; 2005.
11. Wu Y, Wang L, Guo B, Ma PX. Interwoven Aligned Conductive Nanofiber Yarn/Hydrogel Composite Scaffolds for Engineered 3D Cardiac Anisotropy. ACS Nano. 2017; 11(6): 5646-59.
12. Mathur A, Ma Z, Loskill P, Jeeawoody S, Healy KE. *In vitro* cardiac tissue models: Current status and future prospects. Adv Drug Deliv Rev. 2016; 96: 203-13.
13. Gardin C, Ferroni L, Latremouille C, Chachques JC, Mitrečić D, Zavan B. Recent Applications of Three Dimensional Printing in Cardiovascular Medicine. Cells. 2020; 9(3).
14. Stevens A, Lowe JS. Human histology. 3rd ed. Philadelphia: Elsevier/Mosby; 2005.
15. Amann A, Zwierzina M, Koeck S, Gamerith G, Pechriggl E, Huber JM, et al. Development of a 3D angiogenesis model to study tumour - endothelial cell interactions and the effects of anti-angiogenic drugs. Sci Rep. 2017; 7(1): 2963.
16. Hu T, Wu Y, Zhao X, Wang L, Bi L, Ma PX, et al. Micropatterned, electroactive, and biodegradable poly(glycerol sebacate)-aniline trimer elastomer for cardiac tissue engineering. Chemical Engineering Journal. 2019; 366: 208-22.
17. Abedi A, Hasanzadeh M, Tayebi L. Conductive nanofibrous Chitosan/PEDOT:PSS tissue engineering scaffolds. Materials Chemistry and Physics. 2019; 237: 121882.
18. Askari M, Afzali Naniz M, Kouhi M, Saberi A, Zolfagharian A, Bodaghi M. Recent progress in extrusion 3D bioprinting of hydrogel biomaterials for tissue regeneration: a comprehensive review with focus on advanced fabrication techniques. Biomater Sci. 2021; 9(3): 535-73.

19. Qasim M, Haq F, Kang M-H, Kim J-H. 3D printing approaches for cardiac tissue engineering and role of immune modulation in tissue regeneration. Int J Nanomedicine. 2019; 14: 1311-33.
20. Fleischer S, Shapira A, Feiner R, Dvir T. Modular assembly of thick multifunctional cardiac patches. Proc Natl Acad Sci U S A. 2017; 114(8): 1898-903.
21. Engler AJ, Griffin MA, Sen S, Bönnemann CG, Sweeney HL, Discher DE. Myotubes differentiate optimally on substrates with tissue-like stiffness: pathological implications for soft or stiff microenvironments. J Cell Biol. 2004; 166(6): 877-87.
22. Tamadon A, Park K-H, Kim YY, Kang B-C, Ku S-Y. Efficient biomaterials for tissue engineering of female reproductive organs. Tissue Eng Regen Med. 2016; 13(5): 447-54.
23. Chua ILS, Kim H-W, Lee JH. Signaling of extracellular matrices for tissue regeneration and therapeutics. Tissue Eng Regen Med. 2016; 13(1): 1-12.
24. Lutolf MP, Hubbell JA. Synthetic biomaterials as instructive extracellular microenvironments for morphogenesis in tissue engineering. Nat Biotechnol. 2005; 23(1): 47-55.
25. Townsend N, Nichols M, Scarborough P, Rayner M. Cardiovascular disease in Europe--epidemiological update 2015. Eur Heart J. 2015; 36(40): 2696-705.
26. Shen S, Wang H, Qu Y, Huang K, Liu G, Chen Z, et al. Simulating orientation and polarization characteristics of dense fibrous tissue by electrostatic spinning of polymeric fibers. Biomed Opt Express. 2019; 10(2): 571-83.
27. Moorthi A, Tyan Y-C, Chung T-W. Surface-modified polymers for cardiac tissue engineering. Biomater Sci. 2017; 5(10): 1976-87.
28. Shelby Allison, Manuel Ahumada, Cristina Andronic, Brian McNeill, Fabio Variola, May Griffith, et al. Electroconductive nanoengineered biomimetic hybrid fibers for cardiac tissue engineering. J. Mater. Chem. B. 2017; 5(13): 2402-6.
29. Kucinska-Lipka J, Gubanska I, Janik H, Sienkiewicz M. Fabrication of polyurethane and polyurethane based composite fibres by the electrospinning technique for soft tissue engineering of cardiovascular system. Mater Sci Eng C Mater Biol Appl. 2015; 46: 166-76.
30. Falconnet D, Csucs G, Grandin HM, Textor M. Surface engineering approaches to micropattern surfaces for cell-based assays. Biomaterials. 2006; 27(16): 3044-63.
31. Heidi Au HT, Cui B, Chu ZE, Veres T, Radisic M. Cell culture chips for simultaneous application of topographical and electrical cues enhance phenotype of cardiomyocytes. Lab Chip. 2009; 9(4): 564-75.
32. Wang P-Y, Yu J, Lin J-H, Tsai W-B. Modulation of alignment, elongation and contraction of cardiomyocytes through a combination of nanotopography and rigidity of substrates. Acta Biomater. 2011; 7(9): 3285-93.
33. Mohammadi Amirabad L, Massumi M, Shamsara M, Shabani I, Amari A, Mossahebi Mohammadi M, et al. Enhanced Cardiac Differentiation of Human Cardiovascular Disease Patient-Specific Induced Pluripotent Stem Cells by Applying Unidirectional Electrical Pulses Using Aligned Electroactive Nanofibrous Scaffolds. ACS Appl Mater Interfaces. 2017; 9(8): 6849-64.
34. Wang L, Wu Y, Guo B, Ma PX. Nanofiber Yarn/Hydrogel Core–Shell Scaffolds Mimicking Native Skeletal Muscle Tissue for Guiding 3D Myoblast Alignment, Elongation, and Differentiation. ACS Nano. 2015; 9(9): 9167-79.
35. Liu Y, Wang S, Zhang R. Composite poly(lactic acid)/chitosan nanofibrous scaffolds for cardiac tissue engineering. International Journal of Biological Macromolecules. 2017; 103: 1130-7.
36. Kitsara M, Agbulut O, Kontziampasis D, Chen Y, Menasché P. Fibers for hearts: A critical review on electrospinning for cardiac tissue engineering. Acta Biomaterialia. 2017; 48: 20-40.
37. Montgomery M, Ahadian S, Davenport Huyer L, Lo Rito M, Civitarese RA, Vanderlaan RD, et al. Flexible shape-memory scaffold for minimally invasive delivery of functional tissues. Nat Mater. 2017; 16(10): 1038-46.
38. Engelmayr GC, Cheng M, Bettinger CJ, Borenstein JT, Langer R, Freed LE. Accordion-like honeycombs for tissue engineering of cardiac anisotropy. Nat Mater. 2008; 7(12): 1003-10.
39. Kolewe ME, Park H, Gray C, Ye X, Langer R, Freed LE. 3D structural patterns in scalable, elastomeric scaffolds guide engineered tissue architecture. Advanced Materials. 2013; 25(32): 4459-65.
40. M K, C M, C M, AG G, F P, I B, et al. Auxetic Cardiac Patches with Tunable Mechanical and Conductive Properties toward Treating Myocardial Infarction. Adv Funct Mater. 2018; 28(21).
41. Y L, G X, J W, Q W, X L. Cardiomyocyte coculture on layered fibrous scaffolds assembled from micropatterned electrospun mats. Mater Sci Eng C Mater Biol Appl. 2017; 81.
42. Hanley PJ, Young AA, LeGrice IJ, Edgar SG, Loiselle DS. 3-Dimensional configuration of perimysial collagen fibres in rat cardiac muscle at resting and extended sarcomere lengths. The Journal of Physiology. 1999; 517 (Pt 3)(3): 831-7.
43. Jean A, Engelmayr GC. Finite element analysis of an accordion-like honeycomb scaffold for cardiac tissue engineering. Journal of Biomechanics. 2010; 43(15): 3035-43.
44. Zhao G, Zhang X, Lu TJ, Xu F. Recent Advances in Electrospun Nanofibrous Scaffolds for Cardiac Tissue Engineering. Adv. Funct. Mater. 2015; 25(36): 5726-38.
45. Tian F, Hosseinkhani H, Hosseinkhani M, Khademhosseini A, Yokoyama Y, Estrada GG, et al. Quantitative analysis of cell adhesion on aligned micro- and nanofibers. J Biomed Mater Res A. 2008; 84(2): 291-9.
46. Gao H, Shi W, Freund LB. Mechanics of receptor-mediated endocytosis. Proc Natl Acad Sci U S A. 2005; 102(27): 9469-74.
47. Uttayarat P, Toworfe GK, Dietrich F, Lelkes PI, Composto RJ. Topographic guidance of endothelial cells on silicone surfaces with micro- to nanogrooves: orientation of actin filaments and focal adhesions. J Biomed Mater Res A. 2005; 75(3): 668-80.
48. Wang L, Wu Y, Hu T, Guo B, Ma PX. Electrospun conductive nanofibrous scaffolds for engineering cardiac tissue and 3D bioactuators. Acta Biomaterialia. 2017; 59: 68-81.
49. Yadong Tang, Li Liu, Junjun Li, Leqian Yu, Francesco Paolo Ulloa Severino, Li Wang, et al. Effective motor neuron differentiation of hiPSCs on a patch made of crosslinked monolayer gelatin nanofibers. J. Mater. Chem. B. 2016; 4(19): 3305-12.
50. Yadong Tang, Li Liu, Junjun Li, Leqian Yu, Li Wang, Jian Shi, et al. Induction and differentiation of human induced pluripotent stem cells into functional cardiomyocytes on a compartmented monolayer of gelatin nanofibers. Nanoscale. 2016; 8(30): 14530-40.
51. Wang L, Wu Y, Hu T, Ma PX, Guo B. Aligned conductive core-shell biomimetic scaffolds based on nanofiber yarns/hydrogel for enhanced 3D neurite outgrowth alignment and elongation. Acta Biomater. 2019; 96: 175-87.
52. Costa KD, Lee EJ, Holmes JW. Creating alignment and anisotropy in engineered heart tissue: role of boundary conditions in a model three-dimensional culture system. Tissue Eng. 2003; 9(4): 567-77.
53. Black LD, Meyers JD, Weinbaum JS, Shvelidze YA, Tranquillo RT. Cell-induced alignment augments twitch force in fibrin gel-based engineered myocardium via gap junction modification. Tissue Eng Part A. 2009; 15(10): 3099-108.
54. Radisic M, Park H, Shing H, Consi T, Schoen FJ, Langer R, et al. Functional assembly of engineered myocardium by electrical stimulation of cardiac myocytes cultured on scaffolds. Proc Natl Acad Sci U S A. 2004; 101(52): 18129-34.
55. Tandon N, Cannizzaro C, Chao P-HG, Maidhof R, Marsano A, Au HTH, et al. Electrical stimulation systems for cardiac tissue engineering. Nat Protoc. 2009; 4(2): 155-73.
56. Cheema U, Yang S-Y, Mudera V, Goldspink GG, Brown RA. 3-D *in vitro* model of early skeletal muscle development. Cell Motil Cytoskeleton. 2003; 54(3): 226-36.
57. Smith AST, Passey S, Greensmith L, Mudera V, Lewis MP. Characterization and optimization of a simple, repeatable system for the long term *in vitro* culture of aligned myotubes in 3D. J Cell Biochem. 2012; 113(3): 1044-53.
58. Rhim C, Lowell DA, Reedy MC, Slentz DH, Zhang SJ, Kraus WE, et al. Morphology and ultrastructure of differentiating three-dimensional mammalian skeletal muscle in a collagen gel. Muscle Nerve. 2007; 36(1): 71-80.
59. Shin SR, Aghaei-Ghareh-Bolagh B, Gao X, Nikkhah M, Jung SM, Dolatshahi-Pirouz A, et al. Layer-by-layer assembly of 3D tissue constructs with functionalized graphene. Adv Funct Mater. 2014; 24(39): 6136-44.
60. Tijore A, Irvine SA, Sarig U, Mhaisalkar P, Baisane V, Venkatraman S. Contact guidance for cardiac tissue engineering using 3D bioprinted gelatin patterned hydrogel. Biofabrication. 2018; 10(2): 25003.
61. Sean V Murphy, Anthony Atala. 3D bioprinting of tissues and organs. Nat Biotechnol. 2014; 32(8): 773-85.
62. Levato R, Visser J, Planell JA, Engel E, Malda J, Mateos-Timoneda MA. Biofabrication of tissue constructs by 3D bioprinting of cell-laden microcarriers. Biofabrication. 2014; 6(3): 35020.
63. Cui X, Boland T, D'Lima DD, Lotz MK. Thermal inkjet printing in tissue engineering and regenerative medicine. Recent Pat Drug Deliv Formul. 2012; 6(2): 149-55.
64. Saunders RE, Gough JE, Derby B. Delivery of human fibroblast cells by piezoelectric drop-on-demand inkjet printing. Biomaterials. 2008; 29(2): 193-203.
65. Kim JD, Choi JS, Kim BS, Chan Choi Y, Cho YW. Piezoelectric inkjet printing of polymers: Stem cell patterning on polymer substrates. Polymer. 2010; 51(10): 2147-54.
66. Okamoto T, Suzuki T, Yamamoto N. Microarray fabrication with covalent attachment of DNA using bubble jet technology. Nat Biotechnol. 2000; 18(4): 438-41.
67. Goldmann T, Gonzalez JS. DNA-printing: utilization of a standard inkjet printer for the transfer of nucleic acids to solid supports. Journal of Biochemical and Biophysical Methods. 2000; 42(3): 105-10.
68. Takagi D, Lin W, Matsumoto T, Yaginuma H, Hemmi N, Hatada S, et al. High-precision three-dimensional inkjet technology for live cell bioprinting. Int J Bioprint. 2019; 5(2): 208.
69. Xu T, Baicu C, Aho M, Zile M, Boland T. Fabrication and characterization of bio-engineered cardiac pseudo tissues. Biofabrication. 2009; 1(3): 35001.
70. Boland T, Tao X, Damon BJ, Manley B, Kesari P, Jalota S, et al. Drop-on-demand printing of cells and materials for designer tissue constructs. Materials Science and Engineering: C. 2007; 27(3): 372-6.
71. Murphy SV, Skardal A, Atala A. Evaluation of hydrogels for bio-printing applications. J Biomed Mater Res A. 2013; 101(1): 272-84.
72. Khalil S, Sun W. Biopolymer deposition for freeform fabrication of hydrogel tissue constructs. Materials Science and Engineering: C. 2007; 27(3): 469-78.
73. Mironov V, Visconti RP, Kasyanov V, Forgacs G, Drake CJ, Markwald RR. Organ printing: tissue spheroids as building blocks. Biomaterials. 2009; 30(12): 2164-74.

74. Pati F, Jang J, Ha D-H, Won Kim S, Rhie J-W, Shim J-H, et al. Printing three-dimensional tissue analogues with decellularized extracellular matrix bioink. Nat Commun. 2014; 5: 3935.
75. Heinrich MA, Liu W, Jimenez A, Yang J, Akpek A, Liu X, et al. 3D Bioprinting: from Benches to Translational Applications. Small. 2019; 15(23): e1805510.
76. Liu J, Miller K, Ma X, Dewan S, Lawrence N, Whang G, et al. Direct 3D bioprinting of cardiac micro-tissues mimicking native myocardium. Biomaterials. 2020; 256: 120204.
77. Gruijl FR de, van Kranen HJ, Mullenders LHF. UV-induced DNA damage, repair, mutations and oncogenic pathways in skin cancer. Journal of Photochemistry and Photobiology B: Biology. 2001; 63(1-3): 19-27.
78. Chan V, Zorlutuna P, Jeong JH, Kong H, Bashir R. Three-dimensional photopatterning of hydrogels using stereolithography for long-term cell encapsulation. Lab Chip. 2010; 10(16): 2062-70.
79. Lin H, Zhang D, Alexander PG, Yang G, Tan J, Cheng AW-M, et al. Application of visible light-based projection stereolithography for live cell-scaffold fabrication with designed architecture. Biomaterials. 2013; 34(2): 331-9.
80. Atala A, Yoo J. Essentials of 3D biofabrication and translation. Amsterdam: Academic Press; 2015.
81. Jang J, Park H-J, Kim S-W, Kim H, Park JY, Na SJ, et al. 3D printed complex tissue construct using stem cell-laden decellularized extracellular matrix bioinks for cardiac repair. Biomaterials. 2017; 112: 264-74.
82. Jones N. Science in three dimensions: the print revolution. Nature. 2012; 487(7405): 22-3.
83. Chang R, Nam J, Sun W. Effects of dispensing pressure and nozzle diameter on cell survival from solid freeform fabrication-based direct cell writing. Tissue Eng Part A. 2008; 14(1): 41-8.
84. Koti P, Muselimyan N, Mirdamadi E, Asfour H, Sarvazyan NA. Use of GelMA for 3D printing of cardiac myocytes and fibroblasts. J 3D Print Med. 2019; 3(1): 11-22.
85. Lee A, Hudson AR, Shiwarski DJ, Tashman JW, Hinton TJ, Yerneni S, et al. 3D bioprinting of collagen to rebuild components of the human heart. Science. 2019; 365(6452): 482-7.
86. Hinton TJ, Jallerat Q, Palchesko RN, Park JH, Grodzicki MS, Shue H-J, et al. Three-dimensional printing of complex biological structures by freeform reversible embedding of suspended hydrogels. Sci. Adv. 2015; 1(9): e1500758.
87. Madden LR, Mortisen DJ, Sussman EM, Dupras SK, Fugate JA, Cuy JL, et al. Proangiogenic scaffolds as functional templates for cardiac tissue engineering. PNAS. 2010; 107(34): 15211-6.
88. Edri R, Gal I, Noor N, Harel T, Fleischer S, Adadi N, et al. Personalized Hydrogels for Engineering Diverse Fully Autologous Tissue Implants. Adv. Mater. 2018; 31(1): 1803895.
89. Hinton TJ, Hudson A, Pusch K, Lee A, Feinberg AW. 3D Printing PDMS Elastomer in a Hydrophilic Support Bath via Freeform Reversible Embedding. ACS Biomater Sci Eng. 2016; 2(10): 1781-6.
90. Bhattacharjee T, Zehnder SM, Rowe KG, Jain S, Nixon RM, Sawyer WG, et al. Writing in the granular gel medium. Sci Adv. 2015;1(8): e1500655.
91. Noor N, Shapira A, Edri R, Gal I, Wertheim L, Dvir T. 3D Printing of Personalized Thick and Perfusable Cardiac Patches and Hearts. Advanced Science. 2019; 6(11): 1900344.
92. Izadifar M, Babyn P, Kelly ME, Chapman D, Chen X. Bioprinting Pattern-Dependent Electrical/Mechanical Behavior of Cardiac Alginate Implants: Characterization and *Ex Vivo* Phase-Contrast Microtomography Assessment. Tissue Eng Part C Methods. 2017; 23(9): 548-64.
93. Ma X, Dewan S, Liu J, Tang M, Miller KL, Yu C, et al. 3D printed micro-scale force gauge arrays to improve human cardiac tissue maturation and enable high throughput drug testing. Acta Biomater. 2019; 95: 319-27.
94. Ho CMB, Mishra A, Lin PTP, Ng SH, Yeong WY, Kim Y-J, et al. 3D Printed Polycaprolactone Carbon Nanotube Composite Scaffolds for Cardiac Tissue Engineering. Macromolecular Bioscience. 2017; 17(4).
95. Ajdary R, Ezazi NZ, Correia A, Kemell M, Huan S, Ruskoaho HJ, et al. Multifunctional 3D-Printed Patches for Long-Term Drug Release Therapies after Myocardial Infarction. Adv. Funct. Mater. 2020; 30(34): 2003440.
96. Maiullari F, Costantini M, Milan M, Pace V, Chirivì M, Maiullari S, et al. A multi-cellular 3D bioprinting approach for vascularized heart tissue engineering based on HUVECs and iPSC-derived cardiomyocytes. Sci Rep. 2018; 8(1): 13532.
97. Izadifar M, Chapman D, Babyn P, Chen X, Kelly ME. UV-Assisted 3D Bioprinting of Nanoreinforced Hybrid Cardiac Patch for Myocardial Tissue Engineering. Tissue Eng Part C Methods. 2018; 24(2): 74-88.
98. Bejleri D, Streeter BW, Nachlas ALY, Brown ME, Gaetani R, Christman KL, et al. A Bioprinted Cardiac Patch Composed of Cardiac-Specific Extracellular Matrix and Progenitor Cells for Heart Repair. Adv. Healthcare Mater. 2018; 7(23): e1800672.
99. Zhang YS, Arneri A, Bersini S, Shin S-R, Zhu K, Goli-Malekabadi Z, et al. Bioprinting 3D microfibrous scaffolds for engineering endothelialized myocardium and heart-on-a-chip. Biomaterials. 2016; 110: 45-59.
100. Chikae S, Kubota A, Nakamura H, Oda A, Yamanaka A, Akagi T, et al. Three-dimensional bioprinting human cardiac tissue chips of using a painting needle method. Biotechnology and Bioengineering. 2019; 116(11): 3136-42.
101. Panwar A, Tan LP. Current Status of Bioinks for Micro-Extrusion-Based 3D Bioprinting. Molecules. 2016; 21(6).
102. Chimene D, Lennox KK, Kaunas RR, Gaharwar AK. Advanced Bioinks for 3D Printing: A Materials Science Perspective. Ann Biomed Eng. 2016; 44(6): 2090-102.
103. Ouyang L, Highley CB, Rodell CB, Sun W, Burdick JA. 3D Printing of Shear-Thinning Hyaluronic Acid Hydrogels with Secondary Cross-Linking. ACS Biomater. Sci. Eng. 2016; 2(10): 1743-51.
104. Highley CB, Rodell CB, Burdick JA. Direct 3D Printing of Shear-Thinning Hydrogels into Self-Healing Hydrogels. Advanced Materials. 2015; 27(34): 5075-9.
105. Blaeser A, Duarte Campos DF, Puster U, Richtering W, Stevens MM, Fischer H. Controlling Shear Stress in 3D Bioprinting is a Key Factor to Balance Printing Resolution and Stem Cell Integrity. Adv Healthc Mater. 2016; 5(3): 326-33.
106. Moroni L, Burdick JA, Highley C, Lee SJ, Morimoto Y, Takeuchi S, et al. Biofabrication strategies for 3D *in vitro* models and regenerative medicine. Nat Rev Mater. 2018; 3(5): 21-37.
107. Puluca N, Lee S, Doppler S, Münsterer A, Dreßen M, Krane M, et al. Bioprinting Approaches to Engineering Vascularized 3D Cardiac Tissues. Curr Cardiol Rep. 2019; 21(9): 90.
108. Singelyn JM, DeQuach JA, Seif-Naraghi SB, Littlefield RB, Schup-Magoffin PJ, Christman KL. Naturally derived myocardial matrix as an injectable scaffold for cardiac tissue engineering. Biomaterials. 2009; 30(29): 5409-16.
109. Grover GN, Rao N, Christman KL. Myocardial matrix-polyethylene glycol hybrid hydrogels for tissue engineering. Nanotechnology. 2014; 25(1): 14011.
110. Araña M, Gavira JJ, Peña E, González A, Abizanda G, Cilla M, et al. Epicardial delivery of collagen patches with adipose-derived stem cells in rat and minipig models of chronic myocardial infarction. Biomaterials. 2014; 35(1): 143-51.
111. Dai W, Hale SL, Kay GL, Jyrala AJ, Kloner RA. Delivering stem cells to the heart in a collagen matrix reduces relocation of cells to other organs as assessed by nanoparticle technology. Regen Med. 2009; 4(3): 387-95.
112. Ostrovidov S, Salehi S, Costantini M, Suthiwanich K, Ebrahimi M, Sadeghian RB, et al. 3D Bioprinting in Skeletal Muscle Tissue Engineering. Small. 2019; 15(24): e1805530.
113. Pati F, Jang J, Lee JW, Cho D-W. Extrusion Bioprinting. In: Essentials of 3D Biofabrication and Translation: Elsevier; 2015: 123-52.
114. Billiet T, Gevaert E, Schryver T de, Cornelissen M, Dubruel P. The 3D printing of gelatin methacrylamide cell-laden tissue-engineered constructs with high cell viability. Biomaterials. 2014; 35(1): 49-62.
115. Wang Z, Kumar H, Tian Z, Jin X, Holzman JF, Menard F, et al. Visible Light Photoinitiation of Cell-Adhesive Gelatin Methacryloyl Hydrogels for Stereolithography 3D Bioprinting. ACS Appl Mater Interfaces. 2018; 10(32): 26859-69.
116. Toprakhisar B, Nadernezhad A, Bakirci E, Khani N, Skvortsov GA, Koc B. Development of Bioink from Decellularized Tendon Extracellular Matrix for 3D Bioprinting. Macromolecular Bioscience. 2018; 18(10): e1800024.
117. Xu C, Lee W, Dai G, Hong Y. Highly Elastic Biodegradable Single-Network Hydrogel for Cell Printing. ACS Appl Mater Interfaces. 2018; 10(12): 9969-79.
118. Lei Q, He J, Li D. Electrohydrodynamic 3D printing of layer-specifically oriented, multiscale conductive scaffolds for cardiac tissue engineering. Nanoscale. 2019; 11(32): 15195-205.
119. Hu J, Sun X, Ma H, Xie C, Chen YE, Ma PX. Porous nanofibrous PLLA scaffolds for vascular tissue engineering. Biomaterials. 2010; 31(31): 7971-7.
120. Puricel S, Arroyo D, Corpataux N, Baeriswyl G, Lehmann S, Kallinikou Z, et al. Comparison of everolimus- and biolimus-eluting coronary stents with everolimus-eluting bioresorbable vascular scaffolds. J Am Coll Cardiol. 2015; 65(8): 791-801.
121. Pok SW, Wallace KN, Madihally SV. *In vitro* characterization of polycaprolactone matrices generated in aqueous media. Acta Biomater. 2010; 6(3): 1061-8.
122. Aljohani W, Ullah MW, Zhang X, Yang G. Bioprinting and its applications in tissue engineering and regenerative medicine. Int J Biol Macromol. 2018; 107(Pt A): 261-75.
123. Costantini M, Testa S, Mozetic P, Barbetta A, Fuoco C, Fornetti E, et al. Microfluidic-enhanced 3D bioprinting of aligned myoblast-laden hydrogels leads to functionally organized myofibers *in vitro* and *in vivo*. Biomaterials. 2017; 131: 98-110.
124. Griffin M, Castro N, Bas O, Saifzadeh S, Butler P, Hutmacher DW. The Current Versatility of Polyurethane Three-Dimensional Printing for Biomedical Applications. Tissue Eng Part B Rev. 2020; 26(3): 272-83.
125. Feng J, Shi H, Yang X, Xiao S. Self-Adhesion Conductive Sub-micron Fiber Cardiac Patch from Shape Memory Polymers to Promote Electrical Signal Transduction Function. ACS Appl Mater Interfaces. 2021; 13(17): 19593-602.
126. Patrício T, Domingos M, Gloria A, Bártolo P. Characterisation of PCL and PCL/PLA Scaffolds for Tissue Engineering. Procedia CIRP. 2013; 5: 110-4.
127. Ku SH, Lee M, Park CB. Carbon-based nanomaterials for tissue engineering. Adv. Healthcare Mater. 2013; 2(2): 244-60.
128. Cheng Z, Teoh S-H. Surface modification of ultra thin poly (epsilon-caprolactone) films using acrylic acid and collagen. Biomaterials. 2004; 25(11): 1991-2001.
129. Jones DS, Djokic J, McCoy CP, Gorman SP. Poly(ε-caprolactone) and poly(ε-caprolactone)-polyvinylpyrrolidone-iodine blends as ureteral biomaterials: characterisation of mechanical and surface properties, degradation and resistance to encrustation *in vitro*. Biomaterials. 2002; 23(23): 4449-58.

130. Jones DS, McLaughlin DWJ, McCoy CP, Gorman SP. Physicochemical characterisation and biological evaluation of hydrogel-poly(epsilon-caprolactone) interpenetrating polymer networks as novel urinary biomaterials. Biomaterials. 2005; 26(14): 1761-70.
131. Williamson MR, Black R, Kielty C. PCL-PU composite vascular scaffold production for vascular tissue engineering: attachment, proliferation and bioactivity of human vascular endothelial cells. Biomaterials. 2006; 27(19): 3608-16.
132. Chung T-W, Wang Y-Z, Huang Y-Y, Pan C-I, Wang S-S. Poly (epsilon-caprolactone) grafted with nano-structured chitosan enhances growth of human dermal fibroblasts. Artif Organs. 2006; 30(1): 35-41.
133. Colosi C, Shin SR, Manoharan V, Massa S, Costantini M, Barbetta A, et al. Microfluidic Bioprinting of Heterogeneous 3D Tissue Constructs Using Low-Viscosity Bioink. Advanced Materials. 2015; 28(4): 677-84.
134. Zhu K, Shin SR, van Kempen T, Li Y-C, Ponraj V, Nasajpour A, et al. Gold Nanocomposite Bioink for Printing 3D Cardiac Constructs. Adv Funct Mater. 2017; 27(12).
135. Yang Y, Lei D, Huang S, Yang Q, Song B, Guo Y, et al. Elastic 3D-Printed Hybrid Polymeric Scaffold Improves Cardiac Remodeling after Myocardial Infarction. Adv. Healthcare Mater. 2019; 8(10): e1900065.
136. Chen S, Huang T, Zuo H, Qian S, Guo Y, Sun L, et al. A Single Integrated 3D-Printing Process Customizes Elastic and Sustainable Triboelectric Nanogenerators for Wearable Electronics. Adv. Funct. Mater. 2018; 28(46): 1805108.
137. Wang Z, Lee SJ, Cheng H-J, Yoo JJ, Atala A. 3D bioprinted functional and contractile cardiac tissue constructs. Acta Biomater. 2018; 70: 48-56.
138. Haraguchi Y, Shimizu T, Yamato M, Kikuchi A, Okano T. Electrical coupling of cardiomyocyte sheets occurs rapidly via functional gap junction formation. Biomaterials. 2006; 27(27): 4765-74.
139. Noorman M, van der Heyden MAG, van Veen TAB, Cox MGPJ, Hauer RNW, Bakker JMT de, et al. Cardiac cell-cell junctions in health and disease: Electrical versus mechanical coupling. J Mol Cell Cardiol. 2009; 47(1): 23-31.
140. Fujie T, Ahadian S, Liu H, Chang H, Ostrovidov S, Wu H, et al. Engineered nanomembranes for directing cellular organization toward flexible biodevices. Nano Lett. 2013; 13(7): 3185-92.
141. Ramón-Azcón J, Ahadian S, Estili M, Liang X, Ostrovidov S, Kaji H, et al. Dielectrophoretically aligned carbon nanotubes to control electrical and mechanical properties of hydrogels to fabricate contractile muscle myofibers. Advanced Materials. 2013; 25(29): 4028-34.
142. Zanjanizadeh Ezazi N, Ajdary R, Correia A, Mäkilä E, Salonen J, Kemell M, et al. Fabrication and Characterization of Drug-Loaded Conductive Poly(glycerol sebacate)/Nanoparticle-Based Composite Patch for Myocardial Infarction Applications. ACS Appl Mater Interfaces. 2020; 12(6): 6899-909.
143. Wang X, Gu X, Yuan C, Chen S, Zhang P, Zhang T, et al. Evaluation of biocompatibility of polypyrrole *in vitro* and *in vivo*. J Biomed Mater Res A. 2004; 68(3): 411-22.
144. Balint R, Cassidy NJ, Cartmell SH. Conductive polymers: towards a smart biomaterial for tissue engineering. Acta Biomater. 2014; 10(6): 2341-53.
145. O'Neill HS, Gallagher LB, O'Sullivan J, Whyte W, Curley C, Dolan E, et al. Biomaterial-Enhanced Cell and Drug Delivery: Lessons Learned in the Cardiac Field and Future Perspectives. Advanced Materials. 2016; 28(27): 5648-61.
146. KIMES B, BRANDT B. Properties of a clonal muscle cell line from rat heart. Experimental Cell Research, 98(2), 367-381. Experimental Cell Research. 1976; 98(2): 367-81.
147. Hescheler J, Meyer R, Plant S, Krautwurst D, Rosenthal W, Schultz G. Morphological, biochemical, and electrophysiological characterization of a clonal cell (H9c2) line from rat heart. Circ Res. 1991; 69(6): 1476-86.
148. Claycomb WC, Lanson NA, Stallworth BS, Egeland DB, Delcarpio JB, Bahinski A, et al. HL-1 cells: a cardiac muscle cell line that contracts and retains phenotypic characteristics of the adult cardiomyocyte. Proc Natl Acad Sci U S A. 1998; 95(6): 2979-84.
149. Ferrara JLM, Levine JE, Reddy P, Holler E. Graft-versus-host disease. The Lancet. 2009; 373(9674): 1550-61.
150. Badylak SF, Gilbert TW. Immune response to biologic scaffold materials. Semin Immunol. 2008; 20(2): 109-16.
151. Agarwal U, Smith AW, French KM, Boopathy AV, George A, Trac D, et al. Age-Dependent Effect of Pediatric Cardiac Progenitor Cells After Juvenile Heart Failure. Stem Cells Transl Med. 2016; 5(7): 883-92.
152. Takahashi K, Yamanaka S. Induction of pluripotent stem cells from mouse embryonic and adult fibroblast cultures by defined factors. Cell. 2006; 126(4): 663-76.
153. Thomson JA, Itskovitz-Eldor J, Shapiro SS, Waknitz MA, Swiergiel JJ, Marshall VS, et al. Embryonic stem cell lines derived from human blastocysts. Science. 1998; 282(5391): 1145-7.
154. Jang J, Yi H-G, Cho D-W. 3D Printed Tissue Models: Present and Future. ACS Biomater. Sci. Eng. 2016; 2(10): 1722-31.
155. Parikh SS, Blackwell DJ, Gomez-Hurtado N, Frisk M, Wang L, Kim K, et al. Thyroid and Glucocorticoid Hormones Promote Functional T-Tubule Development in Human-Induced Pluripotent Stem Cell-Derived Cardiomyocytes. Circulation research. 2017; 121(12): 1323-30.
156. Kohl P. Heterogeneous Cell Coupling in the Heart. Circ Res. 2003; 93(5): 381-3.
157. Eric Ubil, Jinzhu Duan, Indulekha C. L. Pillai, Manuel Rosa-Garrido, Yong Wu, Francesca Bargiacchi, et al. Mesenchymal–endothelial transition contributes to cardiac neovascularization. Nature. 2014; 514(7524): 585-90.
158. Camelliti P, Borg TK, Kohl P. Structural and functional characterisation of cardiac fibroblasts. Cardiovasc Res. 2005; 65(1): 40-51.
159. Zimmermann W-H, Schneiderbanger K, Schubert P, Didié M, Münzel F, Heubach JF, et al. Tissue engineering of a differentiated cardiac muscle construct. Circ Res. 2002; 90(2): 223-30.
160. Zhang D, Shadrin I, Lam J, Xian H-Q, Snodgrass R, Bursac N. Tissue-engineered Cardiac Patch for Advanced Functional Maturation of Human ESC-derived Cardiomyocytes. Biomaterials. 2013; 34(23): 5813-20.
161. Tandon N, Marsano A, Maidhof R, Wan L, Park H, Vunjak-Novakovic G. Optimization of electrical stimulation parameters for cardiac tissue engineering. J Tissue Eng Regen Med. 2011; 5(6): e115-25.
162. Arai K, Murata D, Verissimo AR, Mukae Y, Itoh M, Nakamura A, et al. Fabrication of scaffold-free tubular cardiac constructs using a Bio-3D printer. PLoS ONE. 2018; 13(12): e0209162.
163. Gaetani R, Doevendans PA, Metz CHG, Alblas J, Messina E, Giacomello A, et al. Cardiac tissue engineering using tissue printing technology and human cardiac progenitor cells. Biomaterials. 2012; 33(6): 1782-90.
164. Park B-W, Jung S-H, Das S, Lee SM, Park J-H, Kim H, et al. *In vivo* priming of human mesenchymal stem cells with hepatocyte growth factor-engineered mesenchymal stem cells promotes therapeutic potential for cardiac repair. Sci Adv. 2020; 6(13): eaay6994.
165. Shixing Huang, Dong Lei, Qi Yang, Yang Yang, Chenyu Jiang, Hongpeng Shi, et al. A perfusable, multifunctional epicardial device improves cardiac function and tissue repair. Nat Med. 2021; 27(3): 480-90.
166. Feinberg AW, Alford PW, Jin H, Ripplinger CM, Werdich AA, Sheehy SP, et al. Controlling the contractile strength of engineered cardiac muscle by hierarchal tissue architecture. Biomaterials. 2012; 33(23): 5732-41.
167. Lind JU, Busbee TA, Valentine AD, Pasqualini FS, Yuan H, Yadid M, et al. Instrumented cardiac microphysiological devices via multimaterial three-dimensional printing. Nat Mater. 2017; 16(3): 303-8.
168. Chou C-L, Rivera AL, Williams V, Welter JF, Mansour JM, Drazba JA, et al. Micrometer scale guidance of mesenchymal stem cells to form structurally oriented large-scale tissue engineered cartilage. Acta Biomater. 2017; 60: 210-9.
169. Salick MR, Napiwocki BN, Sha J, Knight GT, Chindhy SA, Kamp TJ, et al. Micropattern width dependent sarcomere development in human ESC-derived cardiomyocytes. Biomaterials. 2014; 35(15): 4454-64.
170. Bhatia SN, Ingber DE. Microfluidic organs-on-chips. Nat Biotechnol. 2014; 32(8): 760-72.
171. Conant G, Lai BFL, Lu RXZ, Korolj A, Wang EY, Radisic M. High-Content Assessment of Cardiac Function Using Heart-on-a-Chip Devices as Drug Screening Model. Stem Cell Rev Rep. 2017; 13(3): 335-46.
172. Li L, Chen Z, Shao C, Sun L, Sun L, Zhao Y. Graphene Hybrid Anisotropic Structural Color Film for Cardiomyocytes' Monitoring. Adv. Funct. Mater. 2020; 30(3): 1906353.
173. Fu F, Shang L, Chen Z, Yu Y, Zhao Y. Bioinspired living structural color hydrogels. Sci. Robot. 2018; 3(16): eaar8580.
174. Zhou G, Jiang H, Yin Z, Liu Y, Zhang Q, Zhang C, et al. *In Vitro* Regeneration of Patient-specific Ear-shaped Cartilage and Its First Clinical Application for Auricular Reconstruction. EBioMedicine. 2018; 28: 287-302.
175. Raya-Rivera AM, Esquiliano D, Fierro-Pastrana R, López-Bayghen E, Valencia P, Ordorica-Flores R, et al. Tissue-engineered autologous vaginal organs in patients: a pilot cohort study. The Lancet. 2014; 384(9940): 329-36.
176. Zopf DA, Hollister SJ, Nelson ME, Ohye RG, Green GE. Bioresorbable airway splint created with a three-dimensional printer. N Engl J Med. 2013; 368(21): 2043-5.
177. Lovett M, Lee K, Edwards A, Kaplan DL. Vascularization strategies for tissue engineering. Tissue Eng Part B Rev. 2009; 15(3): 353-70.
178. Lee VK, Dai G. Printing of Three-Dimensional Tissue Analogs for Regenerative Medicine. Ann Biomed Eng. 2017; 45(1): 115-31.
179. Fukunishi T, Best CA, Sugiura T, Opfermann J, Ong CS, Shinoka T, et al. Preclinical study of patient-specific cell-free nanofiber tissue-engineered vascular grafts using 3-dimensional printing in a sheep model. J Thorac Cardiovasc Surg. 2017; 153(4): 924-32.
180. Castilho M, Feyen D, Flandes-Iparraguirre M, Hochleitner G, Groll J, Doevendans PAF, et al. Melt Electrospinning Writing of Poly-Hydroxymethylglycolide-co-ε-Caprolactone-Based Scaffolds for Cardiac Tissue Engineering. Adv. Healthcare Mater. 2017; 6(18).
181. Ozbolat IT, Hospodiuk M. Current advances and future perspectives in extrusion-based bioprinting. Biomaterials. 2016; 76: 321-43.
182. Ding Z, Yuan C, Peng X, Wang T, Qi HJ, Dunn ML. Direct 4D printing via active composite materials. Sci Adv. 2017; 3(4): e1602890.
183. Kotikian A, Truby RL, Boley JW, White TJ, Lewis JA. 3D Printing of Liquid Crystal Elastomeric Actuators with Spatially Programed Nematic Order. Advanced Materials. 2018; 30(10).
184. Raviv D, Zhao W, McKnelly C, Papadopoulou A, Kadambi A, Shi B, et al. Active printed materials for complex self-evolving deformations. Sci Rep. 2014; 4: 7422.
185. Gladman AS, Matsumoto EA, Nuzzo RG, Mahadevan L, Lewis JA. Biomimetic 4D printing. Nat Mater. 2016; 15(4): 413-8.
186. Yang H, Leow WR, Wang T, Wang J, Yu J, He K, et al. 3D Printed Photoresponsive Devices Based on Shape Memory Composites. Advanced Materials. 2017; 29(33).
187. Olga Kuksenok, Anna C. Balazs. Stimuli-responsive behavior of composites integrating thermo-responsive gels with photo-responsive fibers. Mater. Horiz. 2015; 3(1): 53-62.

188. Nadgorny M, Xiao Z, Chen C, Connal LA. Three-Dimensional Printing of pH-Responsive and Functional Polymers on an Affordable Desktop Printer. ACS Appl Mater Interfaces. 2016; 8(42): 28946-54.
189. Bodaghi M, Damanpack AR, Liao WH. Adaptive metamaterials by functionally graded 4D printing. Materials & Design. 2017; 135(3): 26-36.
190. Zolfagharian A, Durran L, Gharaie S, Rolfe B, Kaynak A, Bodaghi M. 4D printing soft robots guided by machine learning and finite element models. Sensors and Actuators A: Physical. 2021; 328: 112774.
191. Zolfagharian A, Gregory TM, Bodaghi M, Gharaie S, Fay P. Patient-specific 3D-printed Splint for Mallet Finger Injury. Int J Bioprint. 2020; 6(2): 259.
192. Zolfagharian A, Denk M, Kouzani AZ, Bodaghi M, Nahavandi S, Kaynak A. Effects of Topology Optimization in Multimaterial 3D Bioprinting of Soft Actuators. Int J Bioprint. 2020; 6(2): 260.
193. Urciuolo A, Poli I, Brandolino L, Raffa P, Scattolini V, Laterza C, et al. Intravital three-dimensional bioprinting. Nat Biomed Eng. 2020; 4(9): 901-15.